

Categorization of High-Wind Events and Their Contribution to the Seasonal Breakdown of Stratification on the Southern New England Shelf

Lukas Lobert¹, Glen G. Gawarkiewicz¹, and Albert J. Plueddemann²

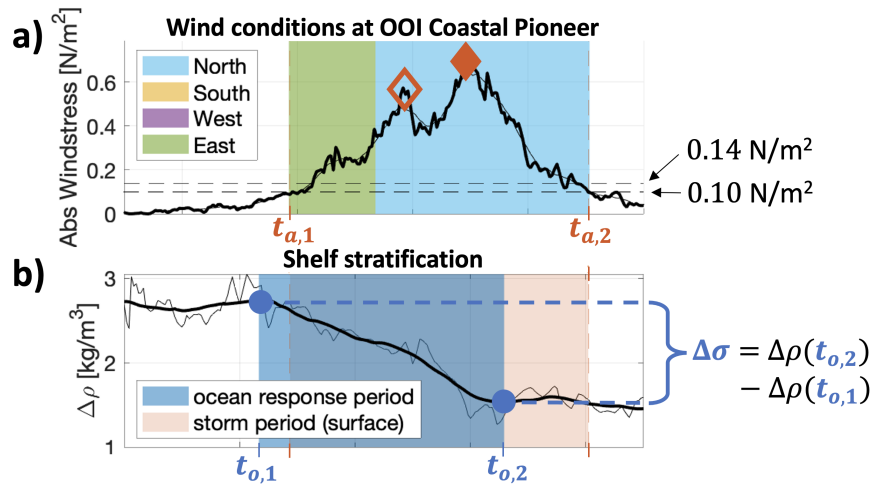
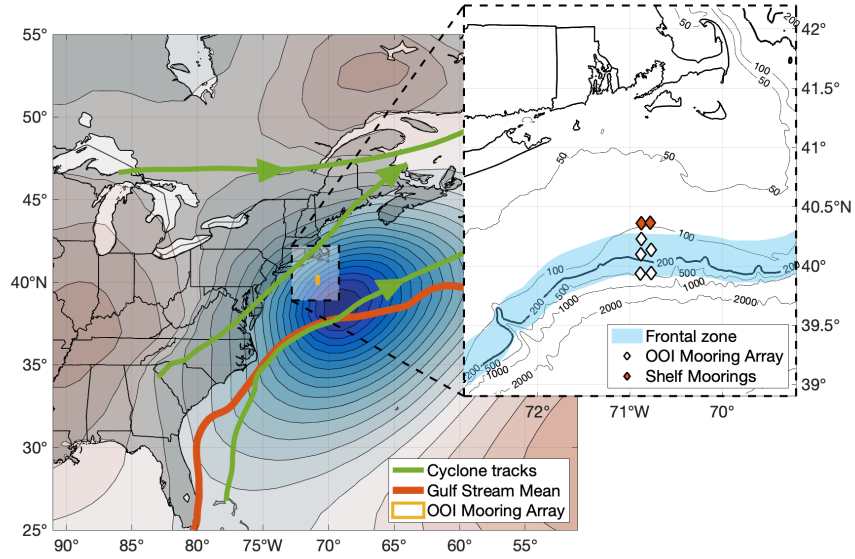
¹Woods Hole Oceanographic Institution

²WHOI

February 27, 2023

Abstract

High-wind events predominantly cause the rapid breakdown of seasonal stratification on the continental shelf. Although previous studies have shown how coastal stratification depends on local wind-forcing characteristics, the locally observed ocean forcing has not yet been linked to regional atmospheric weather patterns that determine the local wind characteristics. Establishing such a connection is a necessary first step towards examining how an altered atmospheric forcing due to climate change affects coastal ocean conditions. Here, we propose a categorization scheme for high-wind events that links atmospheric forcing patterns with changes in stratification. We apply the scheme to the Southern New England shelf utilizing observations from the Ocean Observatories Initiative Coastal Pioneer Array (2015-2022). Impactful wind forcing patterns occur predominantly during early fall, have strong downwelling-favorable winds, and are primarily of two types: i) Cyclonic storms that propagate south of the continental shelf causing strong anticyclonically rotating winds, and ii) persistent large-scale high-pressure systems over eastern Canada causing steady north-easterly winds. These patterns are associated with opposite temperature and salinity contributions to destratification, implying differences in the dominant processes driving ocean mixing. Cyclonic storms are associated with the strongest local wind energy input and drive mechanical mixing and surface cooling. In contrast, steady downwelling-favorable winds from high-pressure systems likely advect salty and less buoyant Slope Water onto the shelf. The high-wind event categorization scheme allows a transition from solely focusing on local wind forcing to considering realistic atmospheric weather patterns when investigating their impact on stratification in the coastal ocean.



1 **Categorization of High-Wind Events and Their**
2 **Contribution to the Seasonal Breakdown of**
3 **Stratification on the Southern New England Shelf**

4 **Lukas Lobert^{1,2}, Glen Gawarkiewicz¹, Albert Plueddemann¹**

5 ¹Woods Hole Oceanographic Institution, Woods Hole, MA, USA

6 ²Massachusetts Institute of Technology, Cambridge, MA, USA

7 **Key Points:**

- 8 • Destratification on the outer shelf occurs predominantly during high-wind events
9 with downwelling-favorable wind forcing during early fall.
- 10 • Cyclones passing south of the shelf and large-scale high-pressure systems over East
11 Canada are most impactful in removing stratification.
- 12 • Differences in the dominant mixing processes likely lead to opposite T/S-contributions
13 to destratification for the impactful wind patterns.

Abstract

High-wind events predominantly cause the rapid breakdown of seasonal stratification on the continental shelf. Although previous studies have shown how coastal stratification depends on local wind-forcing characteristics, the locally observed ocean forcing has not yet been linked to regional atmospheric weather patterns that determine the local wind characteristics. Establishing such a connection is a necessary first step towards examining how an altered atmospheric forcing due to climate change affects coastal ocean conditions. Here, we propose a categorization scheme for high-wind events that links atmospheric forcing patterns with changes in stratification. We apply the scheme to the Southern New England shelf utilizing observations from the Ocean Observatories Initiative Coastal Pioneer Array (2015-2022). Impactful wind forcing patterns occur predominantly during early fall, have strong downwelling-favorable winds, and are primarily of two types: i) Cyclonic storms that propagate south of the continental shelf causing anticyclonically rotating winds, and ii) persistent large-scale high-pressure systems over eastern Canada causing steady north-easterly winds. These patterns are associated with opposite temperature and salinity contributions to destratification, implying differences in the dominant processes driving ocean mixing. Cyclonic storms are associated with the strongest local wind energy input and drive mechanical mixing and surface cooling. In contrast, steady downwelling-favorable winds from high-pressure systems likely advect salty and less buoyant Slope Water onto the shelf. The high-wind event categorization scheme allows a transition from solely focusing on local wind forcing to considering realistic atmospheric weather patterns when investigating their impact on stratification in the coastal ocean.

Plain Language Summary

While coastal waters are strongly density-layered during the summer (called ‘seasonal stratification’), high-wind events during the fall mix the water column and homogenize it. While it is known which local wind conditions tend to mix coastal waters the most, these conditions have not yet been linked to regional atmospheric weather patterns. Drawing such a connection is a necessary step towards understanding how atmospheric climate change may affect the coastal ocean. Here, we propose a categorization scheme to identify which atmospheric patterns have the strongest impact on coastal ocean stratification in the fall. The scheme is applied to the coastal ocean south of New England using seven years of mooring observations. Two weather categories are particularly impactful: Storms passing south of the coastal ocean and large-scale high-pressure systems over eastern Canada. Both categories occur mainly during early fall and bring north-easterly winds associated with the onshore movement of more dense open-ocean water which results in enhanced mixing. Differences in their ocean impact are likely caused by the difference in wind direction steadiness of the two categories. The categorization scheme allows a transition from solely investigating the ocean impacts from local wind forcing to incorporating more realistic atmospheric weather patterns.

1 Level 1 Head: Introduction

The annual cycle of stratification is the dominant mode of variability on the Southern New England continental shelf (abbreviated as SNES and shown in the inset of Fig. 1) on seasonal time scales (Beardsley et al., 1976). The onset and breakdown of stratification marks the transition between two distinct dynamical regimes on the continental shelf and is temporally aligned with blooms in primary production (Schofield et al., 2008) in one of the biologically most productive regions worldwide (O’Reilly & Zetlin, 1998). While the water column is homogenized during winter, surface heating in the spring heats up the surface layer while the interior stays considerably cooler. A seasonal pycnocline forms and reaches its maximum buoyancy gradient in late summer before strat-

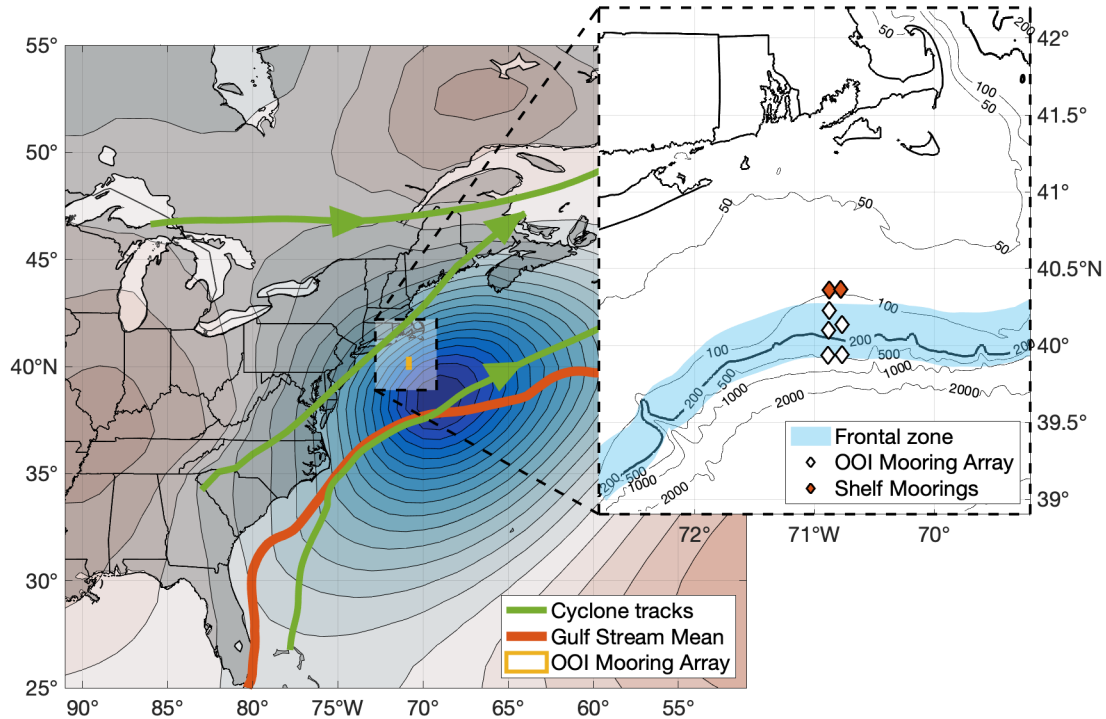


Figure 1. Map of Eastern North America and the Northwest Atlantic with a low-pressure system south of the Southern New England shelf (contours are sea level pressure). Shown are the two dominant cyclone tracks that pass north of the shelf and one cyclone track passing south, circulation features (shelfbreak frontal zone and mean Gulf Stream position), the Southern New England shelf bathymetry, and the location of the OOI Coastal Pioneer Array moorings. Mean storm tracks are derived from manually tracked cyclones during the fall seasons 2015-2021. The mean Gulf Stream position is approximated by the 0.25 cm isoline of the absolute dynamic topography climatological mean (generated using AVISO+ products (AVISO+, 2022)).

64 ification breaks down rapidly during fall (Linder & Gawarkiewicz, 1998). Lentz et al. (2003)
 65 observed that shelf destratification is clustered around storm events, suggesting that seasonal
 66 surface cooling plays a less crucial role than high-wind events.

67 Local wind forcing patterns in the region and their leading-order effects on shelf
 68 stratification are well understood. Northeasterly high-wind forcing during fall is asso-
 69 ciated with rapid destratification (Lentz et al., 2003), following a simple Ekman-forcing
 70 argument for the coastal ocean (Gill, 1982): Steady downwelling-favorable (easterly) winds
 71 are associated with destratification since they advect denser surface water from the Slope
 72 Sea onshore over more buoyant shelf water and can cause enhanced mixing at the shelf-
 73 break due to frontal steepening (shelfbreak frontal zone is shown in Fig. 1). In contrast,
 74 upwelling-favorable winds are typically associated with restratification. Including such
 75 advection processes across the shelfbreak front is necessary to explain the rapidity of the
 76 stratification breakdown on the New Jersey shelf (Forsyth et al., 2018). As their model
 77 study was based significantly further inshore than observations used in this study, an even
 78 larger influence of frontal processes contributing to the observed variability can be ex-
 79 pected on the outer shelf.

80 Even though the leading-order characteristics of wind-driven stratification changes
 81 are well understood, locally observed high-wind forcing on the continental shelf has not
 82 yet been linked to spatio-temporal atmospheric weather patterns. A more comprehen-
 83 sive view of wind-driven ocean forcing is vital to determine which atmospheric forcing
 84 patterns have the strongest impact on shelf stratification. Matching ocean impact with
 85 atmospheric patterns is a necessary first step towards elucidating how the seasonal cy-
 86 cle of stratification on the SNES responds to the changing nature of atmospheric forc-
 87 ing.

88 With climate change affecting wind forcing patterns, the timing of the rapid break-
 89 down of stratification on the continental shelf during fall is likely subject to change. At-
 90 mospheric changes include a northward shift of Northern American storm tracks (Bengtsson
 91 et al. (2006) and Fig. 1) as well as a weaker and wavier polar jet stream due to Arctic
 92 Amplification (Francis & Vavrus, 2012). The boreal jet stream’s waviness increased the
 93 most over North America and the North Atlantic, with the more drastic changes in fall
 94 and winter (Francis & Vavrus, 2015), i.e., the time period of interest for this study.

95 Here, we introduce a categorization scheme based on the spatio-temporal charac-
 96 teristics of high-wind events to identify which atmospheric patterns contribute most to
 97 the annual breakdown of stratification. The approach of categorizing high-wind forcing
 98 patterns to identify differences in the coastal ocean response has been proven success-
 99 ful for the Beaufort Sea continental shelfbreak (Foukal et al., 2019). Scalar metrics, en-
 100 capsulating simplified wind forcing and ocean response variables, allow for easy compar-
 101 ison between events across multiple years of observations. While these simplifying met-
 102 rics cannot capture the full dynamics of a high-wind forcing event, they allow focusing
 103 on the first-order forcing and impact characteristics to determine which events are most
 104 important for the seasonal destratification. By focusing not only on cyclones but on all
 105 types of weather systems associated with high-wind forcing, a more comprehensive un-
 106 derstanding of the factors contributing the most to the seasonal breakdown of ocean strat-
 107 ification in the fall can be gained.

108 Section 2 introduces the data and methods used to identify high-wind events and
 109 their ocean impact on the SNES, followed by section 3 covering the observed interan-
 110 nual variability in destratifying the continental shelf during fall. The spatio-temporal high-
 111 wind event categorization scheme is described in section 4 before section 5 applies the
 112 scheme to distinguish between forcing and ocean impact characteristics. The manner in
 113 which the categorization scheme helps explain the variability of the seasonal impact, event
 114 timing, and mixing contributions are discussed in section 6.

115 **2 Level 1 Head: Data and Methods**

116 **2.1 Level 2 Head: OOI Coastal Pioneer Array**

117 Local atmospheric and subsurface information from the SNES has been recorded
 118 by the inshore moorings of the Ocean Observatories Initiative (OOI) Coastal Pioneer Ar-
 119 ray (abbreviated CP Array and mooring locations marked Fig. 1), a process-oriented shelf-
 120 break observatory in operation between 2015-2022. The CP Array spans across the shelf-
 121 break and is located close to the so-called ‘40/70 benchmark’ at 40°N and 70°W, used
 122 by weather forecasters to estimate winter storm impacts for the US Northeast based on
 123 storm track positions relative to this point (Roller et al., 2016). The CP Array moor-
 124 ings feature surface buoys with meteorological sensors to determine bulk surface fluxes.
 125 Subsurface information is provided through wired profilers with Conductivity-Temperature-
 126 Depth (CTD) sensors in the central water column and fixed instrument packages within
 127 the surface and bottom boundary layers. This combination of assets makes the moor-
 128 ing array well-suited for quantifying high-wind surface forcing impacts on subsurface tem-
 129 perature, salinity, and density structure.

130 Tab. 1 lists the data sources used in this study following the terminology of Gawarkiewicz
 131 and Plueddemann (2020). Technical details about instrumentation and array composi-
 132 tion are provided in their paper. All data are mapped onto an hourly grid, either via av-
 133 eraging (rows 1+3-5) or linear interpolation (row 2). Potential ocean water density (ref-
 134 erenced to $p = 0$) is calculated using TEOS-10 (McDougall & Barker, 2011). Hydrog-
 135 raphy measurements on the shelf are taken at different depths along the 95 m isobath:
 136 Surface, 7 m, continuously between $\sim 30\text{--}70$ m, and 2 m above the bottom. Local wind
 137 and atmospheric data are collected by the CP Array’s three surface buoys, 3 m above
 138 sea level. Surface windstress was computed from wind speed and air density estimates;
 139 occasional data gaps in the Inshore Surface Mooring data were replaced with data from
 140 the Central and Offshore Moorings, respectively. This replacement is justified since the
 141 maximum horizontal distance between the surface buoys (less than 50 km) is much smaller
 142 than the atmospheric synoptic length scale, correlations between surface mooring data
 143 are large ($> 95\%$), lag-correlations peak at zero-lag, and the residual distribution peak
 144 is smaller than the noise.

Table 1. *Data Sources of OOI Coastal Pioneer Array^a time series analyzed in this study.*

#	Variables	Mooring	Platform	Platform depth	Ocean depth
1	T, S	Inshore Surface M. (ISSM)	Surface Buoy	2 m	95 m
2	T, S, P, ρ	Upstr. Inshore Prof. M. (PMUI)	Profiler	$\sim 30 - 70$ m	95 m
3	U, V (wind),	Inshore Surface M. (ISSM)			95 m
4	SLP,	Central Surface M. (CNSM)	Surface Buoy	-3 m	135 m
5	$T_{\text{air}}, \text{RH}$	Offshore Surface M. (OSSM)			450 m

Note. ^afrom Gawarkiewicz and Plueddemann (2020).

145 Since the instrument configuration does not cover the typical depth range of the
 146 seasonal pycnocline (i.e., between 7 and 30 m), mixed-layer depths cannot be estimated.
 147 Instead, a bulk estimate of shelf stratification strength σ is defined as the density dif-
 148 ference $\Delta\rho$ between the shelf interior and the sea surface using data from the inshore moor-
 149 ings:

$$\sigma|_{\text{shelf}} \equiv \Delta\rho|_{\text{shelf}} = \rho(z = 67 \text{ m})|_{\text{PMUI}} - \rho(z = 0 \text{ m})|_{\text{ISSM}}. \quad (1)$$

151 Similar shelf stratification estimates have been used by Forsyth et al. (2018) and Lentz
 152 et al. (2003). The deepest depth of the Upstream Inshore Profiler Mooring range with
 153 consistent data turnout is at $z = 67$ m. According to Linder and Gawarkiewicz (1998)’s
 154 climatology of the shelfbreak front, this depth should be mostly undisturbed from both
 155 variability of the mixed-layer depth and the frontal foot position, making it an appro-
 156 priate location for extracting lower layer density estimates so close to the shelfbreak front.
 157 The (bulk) stratification estimate exploits data from both inshore moorings that are spa-
 158 tially separated by 9.2 km along the same isobath. Since the shelfbreak bathymetry shows
 159 little along-shelf variation across the CP Mooring Array area and the horizontal length
 160 scale of atmospheric weather patterns is much larger than this distance, the horizontal
 161 misalignment is not expected to affect the results.

162 2.2 Level 2 Head: Atmospheric Reanalysis Data

163 Spatial sea level pressure and surface wind data over Northeast America and the
 164 adjacent Atlantic is taken from the ERA5 atmospheric reanalysis data set (Hersbach et
 165 al., 2018). This study utilizes ERA5 data on a $1^\circ \times 1^\circ$ -spatial and 6h-temporal grid. When
 166 comparing ERA5 data with observations from the CP Array’s inshore surface mooring,

167 zonal surface windstress shows a cross-correlation of $r = 0.95$, zero lag-correlation, and
 168 a narrow ($\mathcal{O}(\sigma) = 10^{-2} \text{ N m}^{-2}$) residual distribution with its peak around zero ($\mathcal{O}(\mu) =$
 169 10^{-3} N m^{-2}). Thus, ERA5 data seem trustworthy for the purpose of this study.

170 2.3 Level 2 Head: Connecting surface forcing with subsurface impact

171 This study aims to identify high-wind events and link them with shelf stratifica-
 172 tion changes as a metric for the events' ocean mixing impact. The following algorithm
 173 takes time series of local wind forcing and the previously defined shelf stratification in-
 174 dex as input and outputs a list of individual events and their associated ocean impact.
 175 Event forcing and impact are characterized by a set of simple scalar metrics to allow easy
 176 comparison between events. Fig. 2 applies the algorithm to an exemplary event while
 177 a detailed description is given in the text.

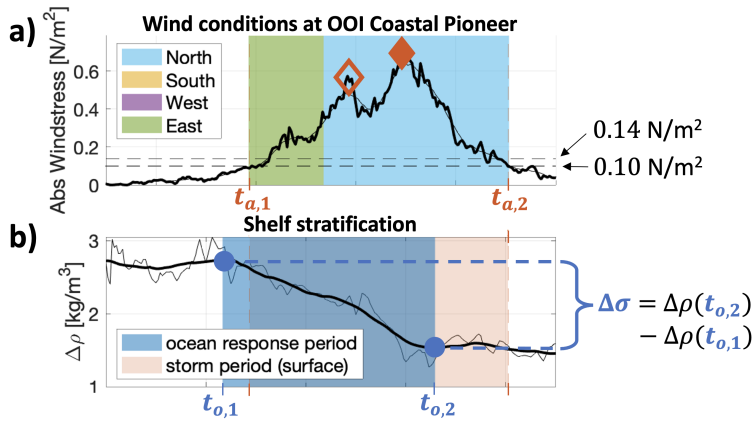


Figure 2. Illustration of how to define a high-wind forcing event, its properties, and sub-surface ocean response using local CP Array time series. a) surface windstress (bold line: 1h resolution data; thin line: 12h-moving mean window). b) stratification estimate (bold line: 36h lowpass-filtered; thin line: 1h resolution data). Diamonds and circles are points of interest identified by the algorithm. The algorithm is explained in the text.

178 Atmospheric high-wind events are defined as peaks above a 0.14 N m^{-2} surface wind-
 179 stress threshold, and both orange diamonds in Fig. 2 represent such peaks. By defin-
 180 ing high-wind events as the absence of calm conditions, the beginning and end of an event
 181 are determined in a two-step process. First, the smoothed surface windstress (thin black
 182 line in Fig. 2a) is examined, and minima are identified on either side of the initial peak
 183 below a threshold of 0.10 N m^{-2} . Secondly, the beginning and end of an event are found
 184 by moving inward from the identified minima until the unsmoothed surface windstress
 185 hits the 0.10 N m^{-2} threshold. The two-step process, including smoothing, ensures that
 186 cyclones whose relatively calm center passes across the CP Array do not get split into
 187 two events. If more than one event peak is associated with the same event time period,
 188 the event gets linked with the more prominent peak (see empty vs. filled orange diamond
 189 in Fig. 2a).

190 Defining the beginning and end of a high-wind event allows for integration of at-
 191 mospheric forcing variables across the event duration, leading to simplified scalar forc-
 192 ing estimates. This study focuses on the integrated along-shelf windstress $\int_{t_{a,1}}^{t_{a,2}} \tau_x dt$ and
 193 the cumulative cubed wind speed $\int_{t_{a,1}}^{t_{a,2}} |U|^3 dt$. Since the x-direction aligns well with the
 194 shelf edge at the location of the CP Array, no coordinate system rotation is required. The
 195 choice of these forcing metrics will be justified in section 6.4. The threshold of 0.14 N m^{-2}

196 represents the upper end of wind force 5 on the Beaufort scale (a little less than 20 knots
 197 winds). The comparatively low threshold ensures that the full bandwidth of impact vari-
 198 ability associated with wind events is captured. Since Forsyth et al. (2018) apply the same
 199 threshold, direct comparison becomes possible. While the chosen threshold affects the
 200 number and duration of identified events, the overall results of this study are robust un-
 201 der reasonable threshold parameter variations.

202 While an event’s windstress peak identifies high-wind event forcing, its leading-order
 203 ocean response is the net change between the pre- and post-event ocean state, i.e., a deriva-
 204 tive variable. The impact of a high-wind event on ocean mixing is quantified by the change
 205 in shelf stratification as measured throughout the event. However, since the ocean re-
 206 sponse may not exactly align with the timing of the locally observed atmospheric forc-
 207 ing, the ocean response time window needs to be determined independently. Fig. 2 il-
 208 lustrates the methodology. An ocean response signal is defined as the stratification esti-
 209 mate difference between two neighboring points of zero slope $\Delta\sigma = \sigma(t_{o,2}) - \sigma(t_{o,1}) =$
 210 $\Delta\rho(t_{o,2}) - \Delta\rho(t_{o,1})$. This simplified approach assumes that the continental shelf is in
 211 steady-state ($\partial_t\sigma = 0$) before and after the event and that the high-wind forcing event
 212 dominates other potential forcing mechanisms that might be present and change the shelf
 213 stratification. We acknowledge the limitations of this assumption, in particular in the
 214 presence of other processes, e.g., other high-wind events in the direct vicinity or shelf-
 215 break frontal instability. However, the large number of observed events allows us to iden-
 216 tify potential outliers where forcing processes could have interacted with one another.
 217 Before identifying zero-slope points, the stratification signal is lowpass-filtered ($\mathcal{O}(36\text{ h})$)
 218 to suppress variability from tidal frequencies, daily cycle harmonics, and internal waves.
 219 This step ensures that irreversible stratification changes are detected on the time scales
 220 associated with synoptic weather events, rather than oscillations occurring at shorter time
 221 scales.

222 Ocean mixing and high-wind forcing events are identified independently before be-
 223 ing matched with each other if they overlap in time. If multiple ocean mixing events over-
 224 lap with a single high-wind event, the wind event is ultimately associated with the larger
 225 absolute stratification difference. The exact start and end points of the ocean response
 226 event have only a weak dependence on the simplified scalar metric of shelf stratification
 227 change, particularly since the data is lowpass-filtered. The algorithm provides a robust
 228 approach to identifying locally observed high-wind forcing events, defining their start and
 229 end, and linking the forcing with its subsurface ocean mixing impact on the outer con-
 230 tinent shelf.

231 **3 Level 1 Head: Seasonal Breakdown of Shelf Stratification**

232 The algorithm described above has been applied to the time series recorded by the
 233 CP Array between May 2015 and 2022 (see fall destratification season 2016 in Fig. 3a+b).
 234 The fall destratification season is defined as the time period of consistent water column
 235 homogenization (Fig. 3c): The start date is set as August 15. The season’s end is the
 236 time at which the lowpass-filtered stratification signal decreases below the rest strati-
 237 fication threshold $\Delta\rho < 1.0\text{ kg m}^{-3}$ and remains there for the rest of the year. The event
 238 that pushes the stratification below the threshold is included in the destratification sea-
 239 son. The 1.0 kg m^{-3} -threshold ensures that late season density fluctuations are not in-
 240 cluded in the analysis. Since smaller thresholds only increase the number of events with
 241 little ocean mixing impact, the overall results of this study are robust to a range of thresh-
 242 olds.

243 The annual cycle of seasonal stratification and shelf homogenization follows the cli-
 244 matology outlined in Linder and Gawarkiewicz (1998) despite noticeable interannual vari-
 245 ability (Fig. 3c). Interannual variability is observed in the timing of re- and destratifi-
 246 cation, the peak stratification during late summer, and the magnitude of the remaining

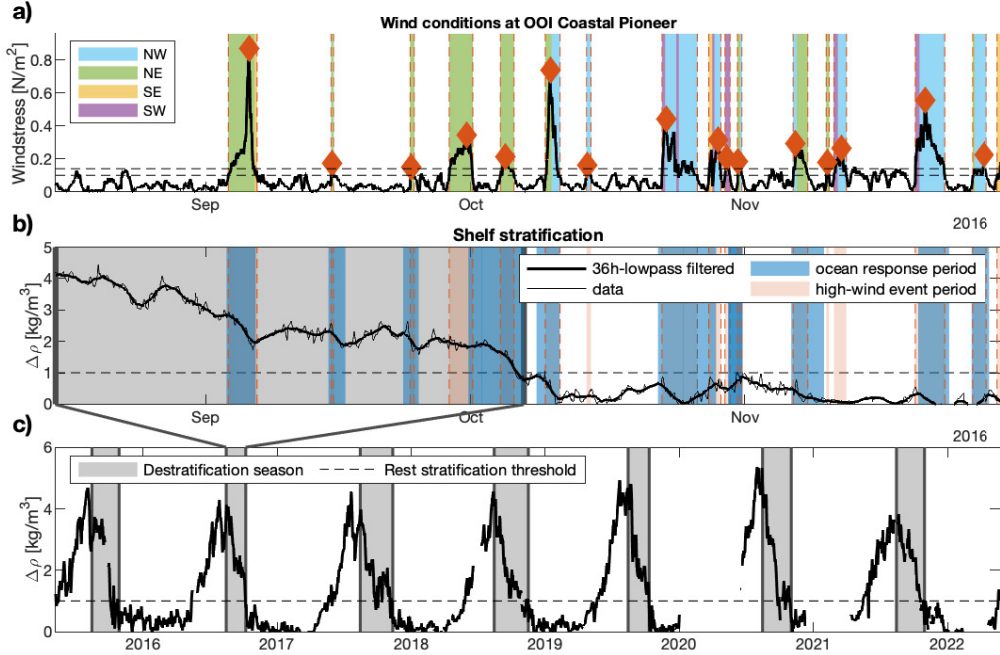


Figure 3. Locally identified high-wind events during fall 2016 and their associated ocean mixing impact by applying the algorithm outlined in section 2.3. a) Surface windstress; main wind directions throughout a high-wind event are color-coded. b) Shelf stratification estimate. Ocean response periods associated with a high-wind event are colored in blue. c) Lowpass-filtered stratification estimate $\Delta\rho$ of full time series (May 2015-2022); de-stratification seasons are colored in grey.

247 stratification and its fluctuations persisting throughout the winter. Stratification reaches
 248 maximum values around mid-August before it rapidly decays to leave the shelf on aver-
 249 age homogenized on October 28 ± 15 days. Tab. 2 lists core information for each de-
 250 stratification season between 2015 and 2021 (left section) and assesses the contribu-
 251 tion of de-stratifying high-wind events to the annual stratification breakdown (right section).
 252 The large interannual variability is depicted in the standard deviations across different
 253 years which tend to be on the same order of magnitude as the mean signals.

254 The net de-stratification from high-wind events alone $\sum_i \Delta\rho_i$ is typically larger than
 255 the initial shelf stratification in late summer (ρ_0) by $35\pm 39\%$ averaged across the seven
 256 years. This result supports Lentz et al. (2003) who inferred from just four storm events
 257 during fall 1996 that the fall de-stratification on the continental shelf is primarily caused
 258 by high-wind forcing and not the cumulative effects from surface cooling throughout the
 259 season. Intermittent re-stratification between high-wind events allows the cumulative ef-
 260 fects from de-stratifying wind events to exceed the initial stratification and prolong the
 261 de-stratification breakdown. Such re-stratification during calm conditions can be caused
 262 by a variety of processes, e.g., surface heating, frontal relaxation, and mixed-layer tur-
 263 bulence. The cumulative change in shelf stratification during calm conditions has a mag-
 264 nitude of $1.3\pm 1.3 \text{ kg m}^{-3}$ per season, i.e., net re-stratification in every but one year. Re-
 265 stratification associated with high-wind events occurs occasionally; though, high-wind
 266 forcing dominantly causes de-stratification.

267 The number of high-wind events per de-stratification season varies widely (see Tab.
 268 2), representing the large variability in the atmospheric forcing on synoptic time scales.

Table 2. *Statistics of fall destratification breakdown on the Southern New England shelf (SNES)*

Year	Destratification season			Destratifying events		
	End	Length	ρ_0	N	$\sum_i^N \Delta\rho_i$	$\overline{\Delta\rho_i}$
2015	Oct 28	74 d	3.7	4	-4.0	-1.0
2016	Oct 07	53 d	4.1	4	-2.8	-0.7
2017	Nov 11	89 d	4.0	12	-7.5	-0.6
2018	Nov 16	93 d	4.3	14	-6.2	-0.5
2019	Oct 11	57 d	4.8	9	-7.6	-0.8
2020	Nov 01	78 d	5.2	10	-7.6	-0.8
2021	Oct 30	76 d	3.8	8	-4.9	-0.6
Mean	Oct 28	74 \pm 15 d	4.3 \pm .5	9 \pm 4	-5.8 \pm 2.0	-0.7 \pm .2

Note. The columns display the year, last day of the destratification season, season length, maximum stratification after August 15, number of destratifying high-wind events during the season, cumulative impact from events, and average impact per event, respectively. The last row presents the mean and standard deviation across all years. Only events associated with destratification are considered. Stratification has units kg m^{-3} .

269 As shown in Fig. 3a, high-wind events during early winter shortly follow upon each other
 270 while they are more sparse during the summer and early fall with large periods of calm
 271 conditions. Hurricanes or their extratropical successors can be particularly impactful if
 272 they pass close to the shelf. Since the North-Atlantic hurricane season peaks in early Septem-
 273 ber, these events typically influence the shelf when stratification is still high. The signal-
 274 to-variability ratio of ocean impact is larger for individual destratifying events than for
 275 the cumulative wind-driven impact across the destratification season. This finding sug-
 276 gests that the timing of the stratification breakdown depends more on the number and
 277 distribution of high-wind events across the season than on the forcing characteristics of
 278 individual events. While each anomaly in the 7-year long data record contains a story
 279 worth telling, this study aims to identify the atmospheric patterns that consistently im-
 280 pact the continental shelf every fall.

281 4 Level 1 Head: Connecting Local Forcing With Regional Patterns

282 This work aims to identify the high-wind event patterns with the largest ocean mix-
 283 ing impact and contribution to the fall stratification breakdown on the continental shelf.
 284 Each local forcing event is part of a large-scale atmospheric pattern with distinct forc-
 285 ing characteristics on the continental shelf. Thus, zooming out and categorizing spatio-
 286 temporal atmospheric patterns allows the partition of the highly variable local forcing
 287 when examining the wind-driven ocean mixing impact. The goal is to determine which
 288 patterns lead to the greatest destratification on the shelf. While section 2.3 provides a
 289 framework to link locally observed wind forcing with its ocean mixing impact, its purely
 290 local approach does not have the ability to differentiate between different atmospheric
 291 patterns.

292 4.1 Level 2 Head: Categorization Scheme for High-Wind Events

293 To link local forcing conditions with atmospheric pattern, a categorization scheme
 294 is established that clusters spatial sea level pressure patterns whenever a high-wind event
 295 gets detected locally by the CP Array. The scheme is motivated by Foukal et al. (2019)'s
 296 approach of investigating the origin of storms that are associated with a downwelling ocean

response on the Alaskan Beaufort Sea continental shelf. Even though the scheme categorizes atmospheric forcing events, it is designed with the oceanographic application of linking the forcing with ocean mixing impacts in mind. Thus, the location of an atmospheric pattern with respect to the SNES is an integral part of the categorization since distance and wind direction largely contribute to the local forcing characteristics.

The high-wind event categorization scheme aims to identify the sea level pressure pattern which is mainly responsible for the locally measured forcing. Pattern clustering, rather than a storm tracking algorithm was used to categorize events since high-wind forcing events on the SNES are caused by a wide variety of types and scales of synoptic weather systems. Conventional storm tracking algorithms are typically trained towards identifying closed-contour cyclone systems (Neu et al., 2013). The pattern clustering relies on human-based decision-making when categorizing high-wind events based on their spatio-temporal characteristics. To minimize human bias, a clear three-step protocol for assigning events to a particular pattern category has been established:

1. **Identification:** Weather systems with closed-contour sea level pressure (SLP) patterns whose isobars reach the CP Array location concurrent with a locally detected wind event (windstress at least 0.14 N m^{-2} at the CP Array) are identified as potential candidates.
2. **Selection:** The candidate weather systems are ranked based on the alignment between their geostrophically induced winds and the locally observed winds during the $\pm 24\text{h}$ period surrounding the local windstress maximum of the event. The weather system with the best alignment gets selected as the one primarily responsible for the locally observed forcing. If there is doubt about the best alignment, the system with the stronger SLP anomaly is selected.
3. **Assignment:** The selected pattern gets assigned to one of the pre-determined categories based on its spatio-temporal characteristics and location with respect to the CP Array. In the rare case that a clear distinction among the categories is not possible, the event remains uncategorized.

Events have been categorized by the same person in a random order to avoid establishing artificial temporal trends.

As typical for unsupervised learning frameworks, the number of categories is not inherent to the dataset and needs to be determined externally. Six categories are sufficient to distinguish between the different locally observed wind forcing patterns while remaining able to unambiguously assign a particular category to an event. While increasing the number of categories would statistically reduce the variability per category, the assignment becomes more ambiguous in reality due to less distinct characteristics of individual categories. While four categories are required to differentiate between the four main wind directions associated with slowly-propagating large-scale patterns, only two categories are required to differentiate between propagating cyclones since storm tracks over New England converge and are mostly oriented in the Northeast direction towards the Icelandic Low (Zielinski & Keim, 2003). Note that there is no separation between tropical and extratropical cyclones. The chosen partitioning of large-scale sea level pressure patterns into the presented four categories is recognizable in the spatial modes and principle component values of an Empirical Orthogonal Function (EOF) analysis (not shown).

4.2 Level 2 Head: Partitioning Weather Systems into Six Spatio-Temporal Categories

Applying the human-centered categorization scheme described above, 98% of all locally observed high-wind events have been assigned to one of six categories. Each category is defined by its distinct sea level pressure (SLP) pattern and named after the lo-

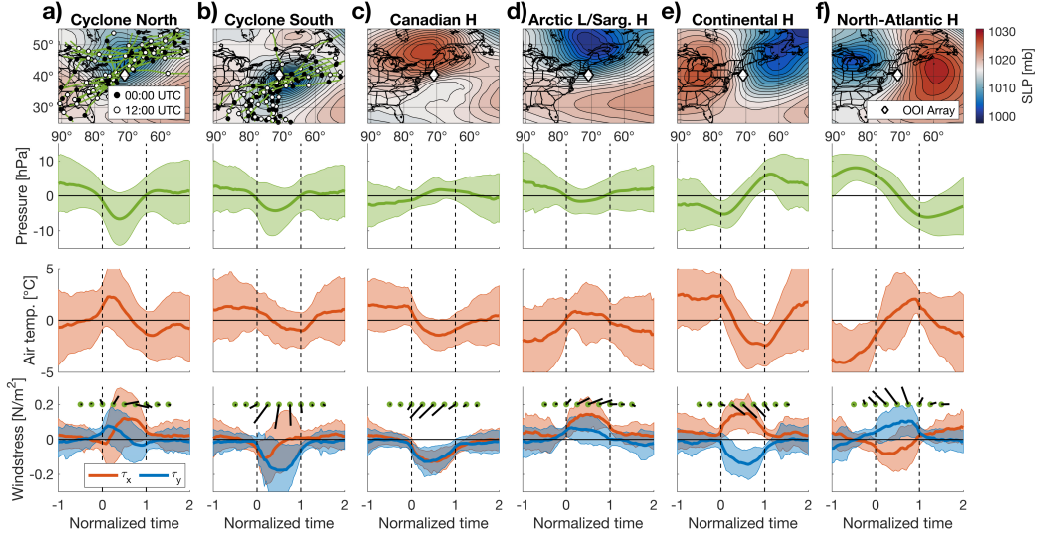


Figure 4. Composites for each high-wind event category (a-f), using categorized high-wind events between May 2015-2022. Row 1: Mean sea level pressure fields at event peaks. Storm tracks (determined manually) are included for all cyclones that occurred during the fall destratification seasons. Row 2-4: Time series composites of sea surface pressure (row 2), surface air temperature (row 3), and surface windstress (row 4) from the continental shelf as observed by the CP Array. Time axis is normalized with the event’s start at $t = 0$ and end at $t = 1$. For better visualization of the wind field, surface windstress vectors (row 4) are shown in black. Time series envelopes represent one-standard deviation.

347 culation of their associated SLP core (Fig. 4). In accordance with geostrophic theory, all
 348 high-wind event categories are associated with strong SLP gradients at the location of
 349 the CP Array at the time of maximum local windstress. The strength of these gradients
 350 is either caused by eastward propagating cyclones/storms with diameters of $\mathcal{O}(100 \text{ km})$
 351 (Fig. 4a+b) or typically more steady large-scale patterns of $\mathcal{O}(1000 \text{ km})$ in spatial extent
 352 (Fig. 4c-f). Cyclones are separated into two categories based on their storm track
 353 with respect to the CP Array and the SNES since the local forcing has opposite wind
 354 directions: *Cyclones North* and *Cyclones South*. Large-scale dipole structures of opposite
 355 SLP anomaly can lead to sufficiently strong SLP gradients between them for gener-
 356 ating high-wind events on the shelf. East-West dipole structures are particularly promi-
 357 nent (Fig. 4e+f) and are named *Continental High* and *North-Atlantic High*. In contrast,
 358 large-scale high- and low-pressure systems north and south of the SNES can cause strong
 359 gradients on the shelf without another system close-by (Fig. 4c+d). They are called *Arc-*
 360 *tic Low/Sargasso High* and *Canadian High*, respectively. There are differences in the sea-
 361 sonal occurrence frequencies between the categories as discussed in section 6.1.

362 While the SLP patterns provide insight into the origin of the locally observed wind
 363 forcing on the continental shelf, the composite time series reveal differences between the
 364 patterns’ temporal forcing development on the SNES. All patterns are associated with
 365 strong changes in SLP which indicate the presence of strong geostrophic winds. While
 366 the first four categories (Fig. 4a-d) describe forcing due to the passage of a weather sys-
 367 tem, the two east-west dipole categories (Fig. 4e+f) reveal that wind forcing can peak
 368 as well between a high and a low pressure system with an enhanced SLP gradient in be-
 369 tween. Abrupt changes in air temperature at an event’s beginning or end suggest that
 370 the high-wind forcing pattern is associated with a frontal passage.

371 The spatio-temporal characteristics of each category lead to distinguishable sur-
 372 face windstress patterns on the SNES. The eastward propagation of the comparatively
 373 small cyclones leads to rotating winds on the continental shelf, and the spatial relation-
 374 ship between the cyclone and the CP Array determines from where the winds come and
 375 how fast they rotate locally. In contrast, large-scale patterns are more stable through-
 376 out the event duration and are associated with more steady winds. Frictional drag in
 377 the surface boundary layer likely causes the deviation between the SLP isobar orienta-
 378 tion at the CP Array location and the windstress vectors towards the low-pressure sys-
 379 tems. While Canadian Highs are associated with steady down-front winds, Arctic Lows/Sargasso
 380 Highs cause steady up-front winds.

381 5 Level 1 Head: High-Wind Event Pattern Characteristics

382 Since the high-wind event categories are associated with different forcing charac-
 383 teristics on the SNES, their average ocean mixing impacts should differ as well. The wind
 384 forcing direction is expected to be crucial for predicting ocean mixing impacts on the con-
 385 tinental shelf due to the existence of a bathymetric boundary (Gill, 1982). Simple scalar
 386 metrics to characterize an event’s wind forcing directionality are the mean wind direc-
 387 tion $\bar{\phi}$ and its standard deviation¹ σ_{ϕ} . A small standard deviation represents steady winds
 388 throughout the event. Following a two-dimensional Ekman theory argument for the coastal
 389 ocean, down-front winds (with the coast to the right on the Northern hemisphere) will
 390 likely cause a downwelling-favorable ocean response. The water transport across the sur-
 391 face Ekman layer will be onshore, causing an opposite flow in the interior to conserve
 392 mass which results in downwelling at the coastal boundary. Up-front winds will cause
 393 the opposite response. Downwelling-favorable (i.e., westward down-front winds) tend to
 394 destratify the shelf by advecting denser slope water onshore at the surface and/or steep-
 395 ening the shelfbreak front, potentially leading to frontal instability and additional shelf-
 396 break exchange (Lentz et al., 2003). The onshore Ekman transport

$$397 \quad V_{Ek} = -\frac{1}{\rho_0 f_0} \tau_x \quad (2)$$

398 solely depends on the along-shelf surface windstress component τ_x . Since the SNES shelf-
 399 break is nearly aligned with the zonal East-West axis, no coordinate system rotation is
 400 required. From Eq. (2), the cumulative (or integrated) zonal surface windstress across
 401 an event $\int_{t_{a,1}}^{t_{a,2}} \tau_x dt$ can act as a first-order estimate for the cross-shelf Ekman forcing.

402 Following the first-order Ekman theory argument outlined above, the cumulative
 403 zonal windstress throughout an event is correlated positively with the associated change
 404 in stratification (Fig. 5a). The observations replicate the trend observed by Forsyth et
 405 al. (2018) in their realistic model study further inshore on the New Jersey shelf (at the
 406 55 m isobath). Downwelling-favorable high-wind events ($\int \tau_x dt < 0$) are associated with
 407 destratification ($\Delta\sigma < 0$) and vice versa. The linear trend is statistically different from
 408 zero on a 99% confidence interval. For the statistical analysis, events have been treated
 409 as independent, which is reasonable since temporal relationships between events are not
 410 preserved. Nonetheless, the spread between Ekman forcing and ocean response remains
 411 large, particularly for positive cumulative Ekman forcing and when treating all high-wind
 412 events alike.

413 The results from the categorization scheme provide additional information about
 414 the individual events, and the categories tend to cluster across the forcing and ocean mix-
 415 ing impact indices. Thus, the categorization allows further distinguishing between dis-
 416 tinct forcing patterns and their influence on stratification (Fig. 5). Both, Canadian Highs
 417 and Cyclones South cause downwelling-favorable winds on the SNES and are consistently

¹ see Eq. (1) in Yamartino (1984)

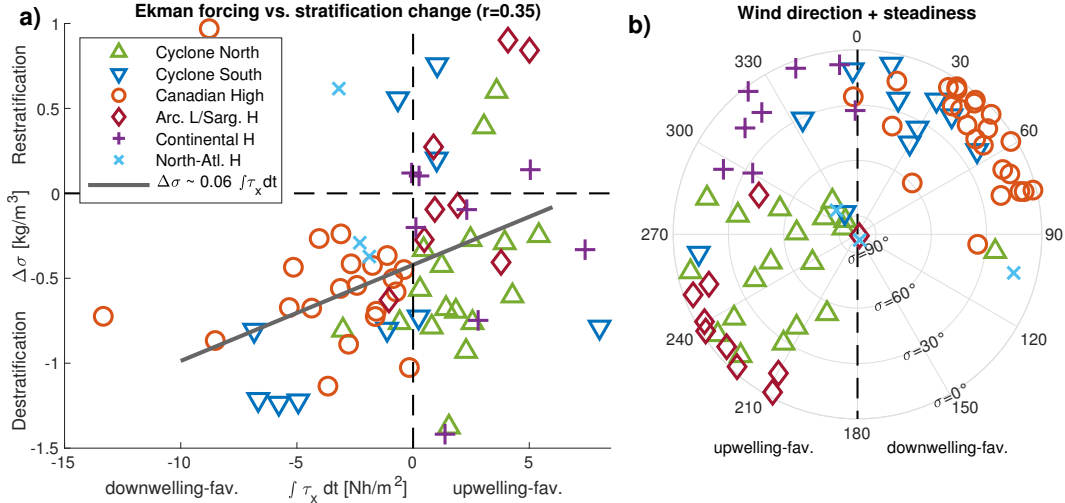


Figure 5. Clustering of high-wind event categories when comparing the local forcing indices with ocean mixing impact for individual events during the fall destratification seasons 2015-2021. a) Cumulative cross-shelf Ekman forcing $\int \tau_x dt$ and stratification change $\Delta\sigma$. The linear trend is a least-squares fit applied to all data shown, while some extreme events are outside the presented axis intervals. b) Leading-order forcing characteristics, including the mean wind direction $\bar{\phi}$ (polar angle of wind origin) and its circular standard deviation σ_ϕ (radial axis); the steadier an event’s wind direction, the further it is away from the origin.

418 associated with destratification. However, their respective clusters differ considerably in
 419 their spread. Canadian Highs cluster closely and show comparatively little variability
 420 in their forcing magnitude, wind direction, and steadiness. Similar forcing conditions co-
 421 incide with relatively little spread in their associated ocean mixing impact. Arctic Lows/Sargasso
 422 Highs describe opposite local wind conditions since they are associated with fairly steady
 423 upwelling-favorable winds. However, these events are not consistently associated with
 424 restratification, potentially since local shear-driven destratification can overcome Ekman-
 425 driven restratification.

426 Cyclone clusters show large variability across all characteristics. Since the forcing
 427 metrics are purely based on local observations at a defined location, the distance and spa-
 428 tial relationship between a cyclone core and the CP Array contribute to the magnitudes
 429 of the established forcing indices. Cyclones take much less time than large-scale weather
 430 systems to pass across distances of the order of their horizontal length scale. In addi-
 431 tion, their distance to the CP Array is more variable than for large-scale weather pat-
 432 terns. Combining these spatial properties likely adds to the enhanced variability in the
 433 local forcing characteristics and reduces the wind direction steadiness throughout the
 434 event. Locally rotating winds throughout the event duration strongly indicate the pas-
 435 sage of Cyclones, and the rotation direction depicts whether the Cyclone passes north
 436 or south of the CP Array.

437 Since East-West dipole patterns have stronger wind components in the cross-shelf
 438 direction, only considering the along-shelf windstress component likely misses important
 439 aspects of the wind forcing. Thus, it is not surprising that East-West dipoles show the
 440 strongest deviation from the linear trend between cumulative along-shelf forcing and ocean
 441 mixing impact (Fig. 5a).

6 Level 1 Head: Discussion

6.1 Level 2 Head: Intra-seasonal Variability in Event Timing

The high-wind event categorization scheme is solely based on the event characteristics throughout the event, i.e., each event is treated as an independent unit while its placement within the annual cycle and potential interaction with other events are not considered. Since the end of the destratification season fluctuates considerably between years (see Tab. 2), the timing of high-wind events likely affects whether they contribute to the fall stratification breakdown or not. In general, a shift from more downwelling-favorable high-wind events early in the fall to more upwelling-favorable high-wind events later in the fall can be observed in most years (see Fig. 3a for 2016). Grouping the high-wind events by category reveals that this observation is indeed caused by differences in the categories' intra-seasonal timing within the fall season (Fig. 6).

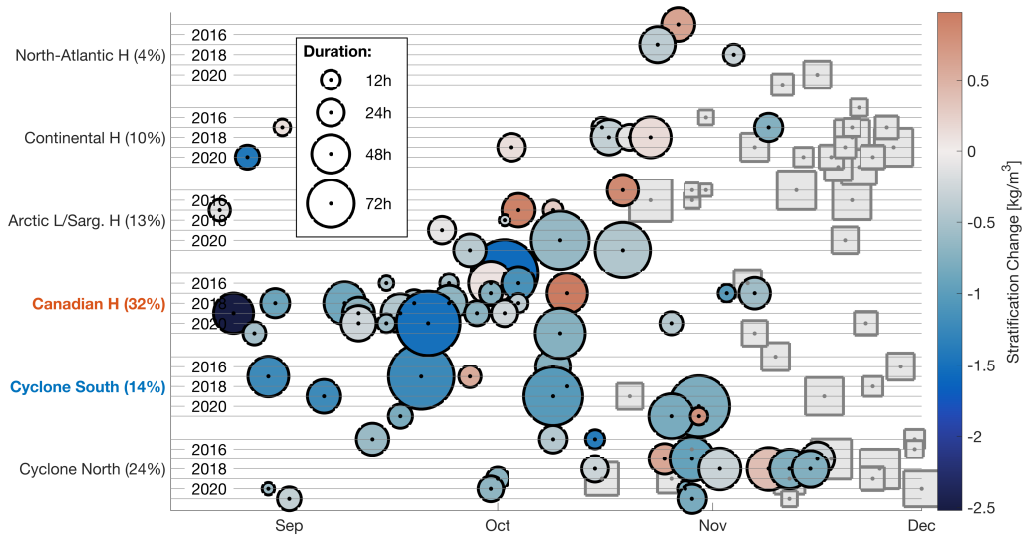


Figure 6. Timing of individual high-wind events within the fall destratification seasons 2015–2021. Events are grouped by category including their frequency of occurrence during the fall destratification (in %). Both, the event duration (marker size) and the associated change in stratification (marker color) are shown. Events that occurred after the stratification breakdown for a given year (see Tab. 2) are shown as grey squares.

Most high-wind event categories cluster on sub-seasonal timescales of roughly 1–2 month length and with sharp edges toward both ends of the distribution. Due to the intermittent nature of high-wind events, seven years of observations are not sufficient to meaningfully determine statistical occurrence distributions. Cyclones South and Canadian Highs tend to occur early in the season, adding to their likelihood to appear in the destratification season. In contrast, East-West dipole patterns and cyclones that propagate further north across New England pick up in late fall/early winter after the stratification breakdown might have already occurred.

Shelf stratification decreases consistently throughout the destratification season, leaving weaker rest stratification for events to affect if they occur late in the season. Thus, the intraseasonal differences in timing between categories might lead to underestimating the ability of individual events late in the destratification season to impact the shelf stratification. However, this work aims to identify the most impactful high-wind weather

467 patterns for the breakdown of seasonal stratification across the whole destratification sea-
 468 son. Both, a high-wind event’s timing and forcing are inherent characteristics of each
 469 high-wind event category, and both variables contribute to the overall seasonal impact
 470 of each category. Thus, disregarding the timing as a characteristic of interest would be
 471 unprofitable for the purpose of this work.

472 6.2 Level 2 Head: Seasonal impact

473 So far, the characteristics of individual high-wind events and their category assign-
 474 ment have been the focus of the analysis. A category’s contribution to the fall stratifi-
 475 cation breakdown is given by combining ocean impact of individual events and the pat-
 476 tern’s occurrence frequency and timing, i.e., $\sum_{i=1}^{N_j} \sigma_{ij} = N_j \cdot \overline{\Delta\sigma_j}$ (total bar height in
 477 Fig. 7a). Here, N_j is the number of events per season in the j -th category and $\overline{\Delta\sigma_j}$ the
 478 average stratification change per event.

479 Cyclones South and Canadian Highs are the most important for the fall stratifi-
 480 cation breakdown on the SNES. Events associated with these categories regularly occur
 481 early in the fall season (Fig. 6) and individual events are consistently associated with
 482 strong destratification (Fig. 5a). Even though Cyclones South, and in particular hur-
 483 ricanes, might be associated with larger individual destratification signals, the contin-
 484 uous presence of multiple Canadian Highs every year makes this event category the num-
 485 ber one contributor to the fall shelf destratification. Events from other high-wind event
 486 categories are occasionally associated with equally strong destratification signals (Fig.
 487 5a). However, their intermittency and the variability in their impact results in less dom-
 488 inant contributions to the average seasonal destratification.

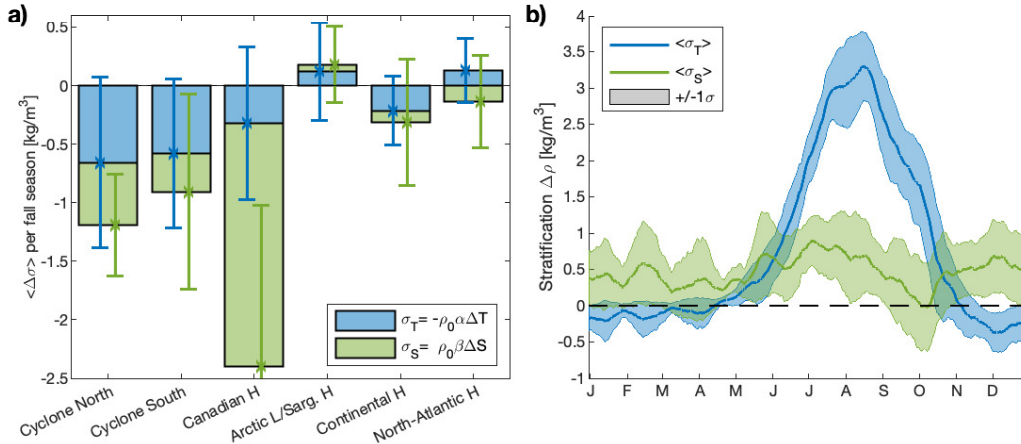


Figure 7. Temperature- (T) and salinity- (S) contributions to stratification on the Southern New England shelf by linearizing the equation of state. a) Cumulative T/S-contributions to the fall stratification breakdown, split by category. b) T/S-contributions to the annual cycle of shelf stratification. The error bars and envelope mark the 1σ -surrounding of interannual variability.

489 The interannual variability of a category’s cumulative contribution to destratifi-
 490 cation is large due to the strong differences in a category’s occurrence between years and
 491 the forcing and impact variability of individual events. On a year-to-year basis signals
 492 can be hidden. Thus, long multi-year time series are vital for investigating the ocean im-
 493 pact of highly variable atmospheric forcing.

6.3 Level 2 Head: Temperature- and Salinity-Contributions to Stratification Changes

High-wind forcing can lead to mixing and destratification on the continental shelf through a variety of processes, and the forcing characteristics determine the relative importance between such mixing processes. The events associated within each high-wind event category, identified based on their spatial sea level pressure patterns, have similar forcing characteristics on the continental shelf (see Figs. 4+5). Thus, similar mixing processes should be present within a category.

Watermasses can be characterized through temperature (T) and salinity (S), which in turn control density and ultimately stratification via the equation of state (EOS). Thus, distinguishing between T- and S-contributions to the observed stratification changes may allow further insight as to the destratification processes at play. Shelf temperature and salinity can be altered by surface heat- and freshwater-fluxes, respectively, advection, entrainment across the pycnocline, and mixing. By linearizing the EOS and proceeding analogous to Eq. 1, the T- and S-contributions to stratification can be estimated as

$$\begin{aligned}\sigma_T \equiv \Delta\rho_T &= -\rho_0\alpha_T\Delta T = -\rho_0\alpha_T [T(z = 67\text{ m}) - T(z = 0\text{ m})] \\ \sigma_S \equiv \Delta\rho_S &= \rho_0\beta_S\Delta S = \rho_0\beta_S [S(z = 67\text{ m}) - S(z = 0\text{ m})]\end{aligned}$$

with the thermal expansion coefficient $\alpha_T(T, S, p) \approx 1.6 \times 10^{-4} \text{ K}^{-1}$, the haline contraction coefficient $\beta_S(T, S, p) \approx 7.6 \times 10^{-4} \text{ PSU}^{-1}$, and an average reference density $\rho_0 = 1025.8 \text{ kg m}^{-3}$. If the shelf heats up, cools, gains salt, and/or freshens non-uniformly across the water column, stratification will change. The net change in T- and S-stratification associated with an individual high-wind event $\Delta\sigma_T$ and $\Delta\sigma_S$ is defined as the difference in stratification throughout the event (analog to section 2.3).

The relative T- and S-contributions to the seasonal destratification differ between different categories with increased interannual variability when distinguishing between T- and S-components instead of focusing on density (Fig. 7). Though, most categories are associated with net destratification on average, seasonal restratification in T and/or S occurs in individual years. Such restratification is less likely for the seasonal T-destratification from Cyclones South and S-destratification from Canadian Highs since the one-sigma error bars do not exceed the multi-year mean signal magnitude.

The initial stratification conditions on the shelf, preceding a high-wind event, likely affect T- and S-contributions to stratification changes. The composition of shelf stratification changes rapidly throughout the destratification season (Fig. 7b). Caused by surface heating during spring and summer, the seasonal stratification is mostly driven by temperature and the seasonal pycnocline typically coincides with the seasonal thermocline (Li et al., 2015). At the end of October, the water column becomes fully temperature-homogenized, and the temperature gradient even reverses with cooler surface temperatures due to surface cooling. Thus, T-destratification becomes less likely for event categories that tend to occur late in the destratification season. In contrast, the S-stratification stays comparatively constant throughout the year since deeper shelf water stays slightly saltier than the surface layer water. However, interannual variability is higher than for temperature, potentially since salinity anomalies are more persistent than temperature anomalies.

Cyclones North, Arctic Lows/Sargasso Highs, and the East-West Dipole patterns cluster later in the destratification season, and S-driven stratification changes are present irrespective of their associated wind directions. In contrast, cyclones that pass south of the continental shelf and Canadian Highs occur early in the season. Nonetheless, they are associated with opposite T/S-signatures of stratification change. The dominance of S-destratification for Canadian Highs exceeds that of any other category. Since timing differences between the two categories are small, differences in the underlying mixing dynamics are likely responsible for the difference.

545 6.4 Level 2 Head: Attribution to dynamical processes

546 Opposite temperature- (T) and salinity- (S) contributions to stratification changes
 547 may act as fingerprints of different destratification processes. Since high-wind forcing char-
 548 acteristics initiate the dynamical ocean response, the observed T/S-fingerprints in the
 549 ocean impact should coincide with differences in the forcing across categories. Both Cy-
 550 clones South and Canadian Highs are associated with downwelling-favorable winds. Nonethe-
 551 less, S-destratification is much more dominant for Canadian Highs.

552 In a horizontally isotropic ocean, the impact of surface forcing on stratification has
 553 been modeled by one-dimensional (1D) mixed-layer theory. Surface windstress causes
 554 shear in the surface boundary layer, leading to instability, mixing, and entrainment of
 555 interior water into the mixed-layer (Price et al., 1986). As a result, the seasonal pyc-
 556 noclone deepens and weakens. As long as ocean currents are negligibly small compared
 557 to the high-wind forcing, impacts are identical irrespective of a category’s wind direc-
 558 tion. The production of turbulent kinetic energy (TKE) from windstress shear $P = -\overline{u'w'} \frac{\partial U}{\partial z} \approx$
 559 $\rho_0^{-1} \tau_x \cdot \frac{\partial U}{\partial z}$ with the horizontal $u = U + u'$ and vertical $w = W + w'$ wind velocity
 560 (mean and fluctuation, respectively) is to first-order proportional to $P \sim |U|^3$ (Niiler
 561 & Kraus, 1977). The integrated $|U|^3$ throughout a high-wind event represents a simpli-
 562 fied estimate for the one-dimensional (1D) mixing potential. Assuming an Osborn-relationship
 563 between the eddy diffusivity K_v and the dissipation ϵ (Osborn, 1980) and neglecting buoy-
 564 ancy and transport terms in the TKE-budget, i.e., $P = \epsilon$, the vertical eddy diffusion
 565 term from shear-induced mixing scales as well with $|U|^3$:

$$566 \quad \mathcal{O}\left(K_v \frac{\partial^2 \rho}{\partial z^2}\right) = \mathcal{O}\left(\Gamma \frac{\epsilon}{N^2} \cdot \frac{\partial^2 \rho}{\partial z^2}\right) \stackrel{P \approx \epsilon}{\approx} \Gamma \cdot \overbrace{\frac{\rho_0^{-1} \tau_x \cdot |U|}{H}}^{\mathcal{O}(P)} \cdot \frac{\Delta \rho}{H^2} = \frac{\Gamma C_D \rho_a}{g H^2} \cdot |U|^3 \quad (3)$$

$$\underbrace{\frac{g \Delta \rho}{\rho_0 H}}_{\mathcal{O}(N^2)}$$

567 with the mixing efficiency Γ , the drag coefficient of wind C_D , air density ρ_a , and verti-
 568 cal length scale H of the pycnocline width and mixed-layer depth (~ 20 m). In the last
 569 step, a bulk formula for the surface windstress $\tau_x = \rho_a C_D U^2$ was applied.

570 The SNES coastline and shelfbreak challenge the 1D mixed-layer theory’s isotropy
 571 assumption. Two-dimensional (2D) Ekman theory applied to the coastal ocean is con-
 572 sistent with observations of de- and restratification based on the wind directionality as
 573 shown in section 5. The cross-shelf Ekman transport is proportional to the along-shelf
 574 surface windstress τ_x and given in Eq. (2). Thus, $|U|^3$ and τ_x are two wind forcing vari-
 575 ables that are representative of two different ocean response mechanisms: 1D mixing from
 576 shear and 2D advection across the shelfbreak, respectively.

577 While Cyclones South and Canadian Highs are both associated with downwelling-
 578 favorable mean winds, differences in their wind direction steadiness and typical wind speeds
 579 lead to deviations between the wind forcing estimates associated with 1D- and 2D-driven
 580 destratification (Fig. 8). The strongest winds on the SNES are caused by a subset of Cy-
 581 clones South, leading to the largest 1D mixing potential estimates $\int_{t_{a,1}}^{t_{a,2}} |U|^3 dt$ from lo-
 582 cal shear production. However, since the cyclones cause comparatively unsteady rotat-
 583 ing winds on the SNES, their cross-shelf Ekman forcing estimate $\int_{t_{a,1}}^{t_{a,2}} \tau_x dt$ does not ex-
 584 ceed that of the Canadian Highs despite their elevated local wind forcing. In contrast,
 585 the Canadian Highs show little variability in their wind direction (Fig. 5b), thus they
 586 tend to line up with the branch representing steady downwelling-favorable zonal wind
 587 forcing. Destratification magnitudes of strong Cyclones South and Canadian Highs are
 588 similar.

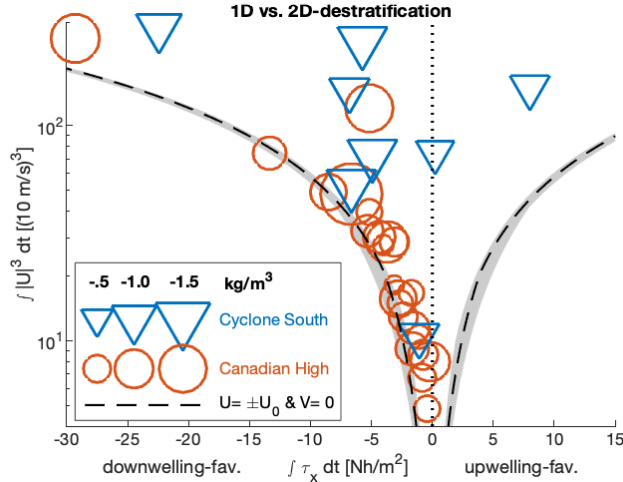


Figure 8. Clustering of Cyclones South and Canadian Highs based on their wind forcing. Y-axis: 1D mixing potential $\int_{a,1}^{a,2} |U|^3 dt$. X-axis: Cross-frontal Ekman forcing, i.e., cumulative zonal surface windstress $\int_{a,1}^{a,2} \tau_x dt$. A fully zonal and steady wind event of average duration would lead to values on the two dashed branches while the grey shading covers the 1-sigma envelope of the distribution of high-wind event duration. Marker size depicts the associated destratification strength.

589 Relating the wind forcing estimates associated with 1D- and 2D-driven destrati-
 590 fication to the shelf/slope hydrography, it can be argued that the two estimates should
 591 be associated with opposite T/S-fingerprints in the stratification changes from high-wind
 592 events. While isotropic mixed-layer theory describes how the 1D mixing potential from
 593 shear production is associated with enhanced surface cooling and entrainment of interior
 594 cold pool water into the summer-heated mixed-layer, the 2D Ekman forcing causes
 595 advection across the shelfbreak. Thus, downwelling-favorable wind forcing causes a surface-
 596 intensified onshore advection of salty slope water onto the shelf while cross-shelf tem-
 597 perature gradients throughout the summer mixed-layer are relatively weak. In an ideal-
 598 ized setting, each forcing process should lead to a different temperature- and salinity-
 599 fingerprint in wind-driven destratification.

600 Applying the T/S-fingerprint concept to the observational record, the spatial clus-
 601 tering of Cyclones South and Canadian Highs in wind forcing space (Fig. 8) aligns well
 602 with the differences in T/S-contributions to stratification changes (Fig. 7): The 1D mix-
 603 ing potential magnitudes are the strongest for Cyclones South that are associated with
 604 T-driven destratification while 2D Ekman advection is expected to lead to S-driven de-
 605 stratification. Canadian Highs show such a forcing and ocean response behavior. Fur-
 606 ther analysis of the velocity fields and cross-shelf gradients would be required to allow
 607 a direct comparison between contributions from the two forcing processes in a 2D cross-
 608 shelf framework. Unresolved 3D processes from along-shelf gradients and frontal oscil-
 609 lations/instabilities continue to add to the variability.

610 6.5 Level 2 Head: Frontal Pre-Conditioning

611 Fingerprints of different forcing processes in the shelf stratification signal have been
 612 motivated theoretically and rely on spatial gradients. For example, the simple 2D Ekman-
 613 argument to explain the shelf stratification's sensitivity to steady downwelling-favorable
 614 winds, and the influx of high-salinity offshore water relies on cross-frontal density gra-

615 dients across the shelfbreak. The shelfbreak front south of New England consistently sep-
 616 arates cooler and fresher continental shelf water from warmer and saltier Slope Sea wa-
 617 ter, leading to the strongest horizontal density gradients in the region. However, these
 618 gradients have not yet been considered despite the CP Array’s proximity to the front.
 619 In the climatological mean, the frontal jet core is at the 200 m-isobath (Linder & Gawarkiewicz,
 620 1998), while the CP Array’s inshore moorings measure around the 95 m-isobath. The shelf-
 621 break front is inherently unstable (e.g., Flagg and Beardsley (1978); Gawarkiewicz and
 622 Chapman (1991); Lozier et al. (2002)), leading to ubiquitous meandering and frontal ed-
 623 dies on top of an annual cycle of varying frontal strength.

624 Frontal pre-conditioning describes the hypothesis that the physical state of the shelf-
 625 break front preceding a high-wind forcing event affects the wind-driven shelf mixing and
 626 needs to be included to quantitatively assess the contribution of different forcing pro-
 627 cesses to destratification. Variability in the frontal state likely adds to the spread ob-
 628 served when comparing the wind forcing with an event’s impact on stratification (Fig.
 629 5a). The data record reveals that large stratification changes are regularly associated with
 630 rapid changes in temperature and salinity across the water column (not shown). Since
 631 the magnitudes of typical surface buoyancy forces are insufficient to explain such obser-
 632 vations, onshore advection of the shelfbreak front across the mooring position likely cause
 633 these anomalies. Various wind-driven cross-frontal exchange processes have been iden-
 634 tified (Houghton et al., 1988; Gawarkiewicz et al., 1996; Mahadevan et al., 2010), and
 635 the CP Array is well designed to assess frontal pre-conditioning and shelfbreak exchange
 636 events in the future.

637 7 Level 1 Head: Conclusion

638 Atmospheric high-wind forcing events and their impact on ocean stratification on
 639 the Southern New England shelf (SNES) have been investigated to identify which high-
 640 wind event patterns contribute most to the rapid breakdown of stratification during the
 641 fall. The variability in the timing of the stratification breakdown is large (± 15 days) and
 642 likely depends more on the number and distribution of high-wind events across the sea-
 643 son than on the individual forcing characteristics.

644 A high-wind categorization scheme has been developed to group weather events into
 645 six categories based on their spatio-temporal sea-level pressure signal and locally observed
 646 wind field on the SNES. Mean composites capture the distinct forcing characteristics in-
 647 herent with each category. Two event categories are particularly impactful for the sea-
 648 sonal stratification breakdown: Cyclones that pass south of the SNES (*Cyclones South*)
 649 and high-pressure systems over eastern Canada (*Canadian Highs*) tend to occur during
 650 early fall and are associated with downwelling-favorable winds on the SNES. This result
 651 is in good accordance with Ekman theory for the coastal ocean (Gill, 1982) and provides
 652 an observation-based measure of interannual variability for the first time.

653 Cyclones are the most ubiquitous high-wind event pattern in the extratropics. How-
 654 ever, cyclones noticeably deviate from the idealized Ekman theory case since local wind
 655 vectors tend to continuously rotate throughout a cyclone’s passage. As a result, their
 656 Ekman cross-shelf circulation cell should be less pronounced than for the steady Cana-
 657 dian Highs. The Canadian Highs establish a real-life representation of the idealized downwelling-
 658 favorable Ekman-forcing case on the SNES since the wind forcing is relatively steady through-
 659 out the event. Thus, while the strong wind speeds associated with Cyclones South have
 660 notable impact on local vertical mixing, Canadian Highs produce a similar strong ocean
 661 response with weaker, steadier winds. In addition, their ocean response more likely ex-
 662 tends the high-wind forcing duration due to enhanced horizontal advection, post-event
 663 restratification, and frontal relaxation.

664 Differences in mixing processes associated with Cyclones and Canadian Highs are
 665 suggested by the opposite temperature- (T) and salinity- (S) contributions to the wind-
 666 driven shelf destratification. Cyclones South are associated with larger T-destratification,
 667 likely due to their intense wind speeds leading to enhanced local mixing, cold pool wa-
 668 ter entrainment, and turbulent surface cooling. In contrast, Canadian Highs are weaker;
 669 however, their secondary Ekman circulation in the cross-shelf direction causes enhanced
 670 S-destratification. Frontal pre-conditioning by the nearby shelfbreak front likely adds to
 671 the observed variability in wind-driven ocean impact and should be included to quan-
 672 tify the contribution of cross-shelf exchange processes to destratification on the shelf.

673 The categorization scheme has shifted the focus from solely interpreting local wind
 674 forcing on the continental shelf to studying the ocean impacts of realistic spatio-temporal
 675 atmospheric weather patterns. Since local conditions are the product of large-scale weather
 676 systems potentially affected by climate change, the categorization results are a first step
 677 towards exploring how climate change trends may affect the atmospheric ocean-forcing
 678 and contribute to the immense environmental pressure on the New England ecosystem
 679 (Pinsky et al., 2013). For example, it is well established that enhanced polar jet stream
 680 variability leads to more persistent weather patterns in the mid-latitudes (Francis & Vavrus,
 681 2012), and Chen et al. (2014) have established the impacts of jetstream anomalies on the
 682 SNES and beyond.

683 8 Open Research

684 The results from the high-wind event categorization scheme and storm tracking can
 685 be found at² <https://tinyurl.com/34aym8z5>, including all high-wind events observed
 686 by the OOI Coastal Pioneer Array (05/2019-11/2022), local forcing and ocean response
 687 metrics, and the categorization results using spatio-temporal event characteristics. This
 688 work heavily relies on bulk meteorological and subsurface observations from the OOI Coastal
 689 Pioneer Array to assess local wind-forcing conditions and stratification changes on the
 690 SNES. Data is publically available through multiple gateways, e.g., through the Data Ex-
 691 plorer ERDDAP server erddap.dataexplorer.oceanobservatories.org (NSF Ocean
 692 Observatory Initiative, 2022). Registration is required for download. ERA5 hourly data
 693 on single levels was downloaded from the Copernicus Climate Change Service (C3S) Cli-
 694 mate Data Store (doi.org/10.24381/cds.adbb2d47) and been used to gain spatio-temporal
 695 information on high-wind event patterns (Hersbach et al., 2018). Registration is required
 696 for download. The mean Gulf Stream position was estimated from the the Monthly Cli-
 697 matology maps of Mean Absolute Dynamic Topography (MADT-H) for 1993-2020, a global
 698 gridded ($1/4^\circ \times 1/4^\circ$) Ssalto/Duacs data product distributed in delayed time by AVISO+.
 699 Data is available through multiple gateways upon registration, e.g., through the Thredds
 700 data server (AVISO+, 2022). Thermodynamic properties of seawater have been deter-
 701 mined by using the Gibbs-SeaWater (GSW) Oceanographic Toolbox (McDougall & Barker,
 702 2011), Version 3.06.12, available via teos-10.org/software.htm.

703 Acknowledgments

704 We are grateful for financial support from the German Federal Ministry for Eco-
 705 nomic Affairs and Climate Action’s ERP scholarship fund (LL), grants N00014-21-1-2559
 706 and N00014-19-1-2646 from the Office of Naval Research (GG), and the Scripps Chair
 707 for Excellence in Oceanography (AL). We thank Paula Fratantoni for enriching discus-
 708 sions during the early phase of the project. Paula Fratantoni and Svenja Ryan provided
 709 valuable comments on the manuscript. Observations are provided by the Ocean Obser-

² Permanent object identifier/zotero-doi will follow after peer-review and replace the currently provided link.

710 vatories Initiative (OOI), which is a major facility fully funded by the National Science
 711 Foundation under Cooperative Agreement No. 1743430. The results contain modified
 712 Copernicus Climate Change Service information, 2022. The Ssalto/Duacs altimeter prod-
 713 ucts were produced and distributed by the Copernicus Marine and Environment Mon-
 714 itoring Service (CMEMS) (<http://www.marine.copernicus.eu>).

715 References

- 716 AVISO+. (2022). Ssalto/Duacs gridded Mean Absolute Dynamic Topography
 717 (MADT-H) Monthly Climatology product (1993-2020). [Dataset] *Thredds*
 718 *Data Server*. Retrieved 2022-12-23, from [tds.avisio.altimetry.fr/
 719 thredds/catalog/dataset-duacs-climatology-global/delayed-time/
 720 monthly_clim/madt_h/catalog.html](https://tds.avisio.altimetry.fr/thredds/catalog/dataset-duacs-climatology-global/delayed-time/monthly_clim/madt_h/catalog.html)
- 721 Beardsley, R., Boicourt, W., & Hansen, D. (1976). Middle Atlantic continental shelf
 722 and New York Bight. In M. Cross (Ed.), *Special symposia* (Vol. 2, p. 20-34).
 723 American Society of Limnology and Oceanography.
- 724 Bengtsson, L., Hodges, K. I., & Roeckner, E. (2006). Storm Tracks and Climate
 725 Change. *Journal of Climate*, *19*(15), 3518 - 3543. doi: 10.1175/JCLI3815.1
- 726 Chen, K., Gawarkiewicz, G., Lentz, S. J., & Bane, J. M. (2014). Diagnosing the
 727 warming of the Northeastern U.S. Coastal Ocean in 2012: A linkage between
 728 the atmospheric jet stream variability and ocean response. *Journal of Geophys-
 729 ical Research: Oceans*, *119*(1), 218-227. doi: 10.1002/2013JC009393
- 730 Flagg, C. N., & Beardsley, R. C. (1978). On the stability of the shelf water/slope
 731 water front south of New England. *Journal of Geophysical Research: Oceans*,
 732 *83*(C9), 4623-4631. doi: 10.1029/JC083iC09p04623
- 733 Forsyth, J., Gawarkiewicz, G., Andres, M., & Chen, K. (2018). The Interan-
 734 nual Variability of the Breakdown of Fall Stratification on the New Jersey
 735 Shelf. *Journal of Geophysical Research: Oceans*, *123*(9), 6503-6520. doi:
 736 10.1029/2018JC014049
- 737 Foukal, N. P., Pickart, R. S., Moore, G. W. K., & Lin, P. (2019). Shelfbreak down-
 738 welling in the Alaskan Beaufort Sea. *Journal of Geophysical Research: Oceans*,
 739 *124*(10). doi: 10.1029/2019JC015520
- 740 Francis, J. A., & Vavrus, S. J. (2012). Evidence linking Arctic amplification to ex-
 741 treme weather in mid-latitudes. *Geophysical Research Letters*, *39*(6), L06801.
 742 doi: 10.1029/2012GL051000
- 743 Francis, J. A., & Vavrus, S. J. (2015). Evidence for a wavier jet stream in response
 744 to rapid Arctic warming. *Environmental Research Letters*, *10*(1), 014005. doi:
 745 10.1088/1748-9326/10/1/014005
- 746 Gawarkiewicz, G., & Chapman, D. C. (1991). Formation and Maintenance of
 747 Shelfbreak Fronts in an Unstratified Flow. *Journal of Physical Oceanography*,
 748 *21*(8), 1225 - 1239. doi: 10.1175/1520-0485(1991)021(1225:FAMOSF)2.0.CO;
 749 2
- 750 Gawarkiewicz, G., Linder, C. A., Lynch, J. F., Newhall, A. E., & Bisagni, J. J.
 751 (1996). A surface-trapped intrusion of slope water onto the continental shelf in
 752 the Mid-Atlantic Bight. *Geophysical Research Letters*, *23*(25), 3763-3766. doi:
 753 10.1029/96GL03427
- 754 Gawarkiewicz, G., & Plueddemann, A. (2020). Scientific rationale and concep-
 755 tual design of a process-oriented shelfbreak observatory: the OOI Pi-
 756 oneer Array. *Journal of Operational Oceanography*, *13*(1), 19-36. doi:
 757 10.1080/1755876X.2019.1679609
- 758 Gill, A. (1982). Atmosphere-Ocean Dynamics. In *International geophysics series*
 759 (Vol. 30). Academic Press.
- 760 Hersbach, H., Bell, B., Berrisford, P., Biavati, G., Horányi, A., Muñoz Sabater, J.,
 761 ... Thépaut, J.-N. (2018). ERA5 hourly data on single levels from 1959 to
 762 present. *Copernicus Climate Change Service (C3S) Climate Data Store (CDS)*.

- doi: 10.24381/cds.adbb2d47
- Houghton, R., Aikman, F., & Ou, H. (1988). Shelf-slope frontal structure and cross-shelf exchange at the New England shelf-break. *Continental Shelf Research*, 8(5), 687 - 710. doi: 10.1016/0278-4343(88)90072-6
- Lentz, S., Shearman, K., Anderson, S., Plueddemann, A., & Edson, J. (2003). Evolution of stratification over the New England shelf during the Coastal Mixing and Optics study, August 1996–June 1997. *Journal of Geophysical Research*, 108(C1). doi: 10.1029/2001JC001121
- Li, Y., Fratantoni, P. S., Chen, C., Hare, J. A., Sun, Y., Beardsley, R. C., & Ji, R. (2015). Spatio-temporal patterns of stratification on the Northwest Atlantic shelf. *Progress in Oceanography*, 134, 123-137. doi: 10.1016/j.pocean.2015.01.003
- Linder, C. A., & Gawarkiewicz, G. (1998). A climatology of the shelfbreak front in the Middle Atlantic Bight. *Journal of Geophysical Research*, 103(C9), 18405–18423. doi: 10.1029/98JC01438
- Lozier, M. S., Reed, M. S. C., & Gawarkiewicz, G. (2002). Instability of a Shelfbreak Front. *Journal of Physical Oceanography*, 32(3), 924 - 944. doi: 10.1175/1520-0485(2002)032<0924:IOASF>2.0.CO;2
- Mahadevan, A., Tandon, A., & Ferrari, R. (2010). Rapid changes in mixed layer stratification driven by submesoscale instabilities and winds. *Journal of Geophysical Research: Oceans*, 115(C3). doi: 10.1029/2008JC005203
- McDougall, T., & Barker, P. (2011). Getting started with TEOS-10 and the Gibbs Seawater (GSW) Oceanographic Toolbox. (SCOR/IAPSO WG 127), 28pp. Retrieved 2020-05-25, from <https://hadoop.apache.org>
- Neu, U., Akperov, M. G., Bellenbaum, N., Benestad, R., Blender, R., Caballero, R., ... Wernli, H. (2013). IMILAST: A Community Effort to Intercompare Extratropical Cyclone Detection and Tracking Algorithms. *Bulletin of the American Meteorological Society*, 94(4), 529 - 547. doi: 10.1175/BAMS-D-11-00154.1
- Niiler, P., & Kraus, E. (1977). One-dimensional models of the upper ocean. In E. B. Kraus (Ed.), *Modelling and prediction of the upper layers of the ocean* (p. 143-172). Pergamon.
- NSF Ocean Observatory Initiative. (2022). Bulk Meteorology Instrument Package (METBK) and CTD (cp03issm-sbd11-06-metbka000, cp01cnsm-sbd11-06-metbka000, cp01cnsm-sbd12-06-metbka000, cp04ossm-sbd11-06-metbka000, cp03issm-rid27-03-ctdbpc000, cp02pmui-wfp01-03-ctdpfk000) data from Pioneer NES Array from 2015-05-09 to 2022-06-01. [Dataset] *Data Explorer ERDDAP*. Retrieved 2022-06-17, from erddap.oceanobservatories.org
- O'Reilly, J., & Zetlin, C. (1998). *Seasonal, Horizontal, and Vertical Distribution of Phytoplankton Chlorophyll a in the Northeast U.S. Continental Shelf Ecosystem* (Tech. Rep.). U.S. Department of Commerce. NOAA Tech. Rep. NMFS 139.
- Osborn, T. R. (1980). Estimates of the Local Rate of Vertical Diffusion from Dissipation Measurements. *Journal of Physical Oceanography*, 10(1), 83 - 89. doi: 10.1175/1520-0485(1980)010<0083:EOTLRO>2.0.CO;2
- Pinsky, M. L., Worm, B., Fogarty, M. J., Sarmiento, J. L., & Levin, S. A. (2013). Marine taxa track local climate velocities. *Science*, 341(6151), 1239–1242. doi: 10.1126/science.1239352
- Price, J. F., Weller, R. A., & Pinkel, R. (1986). Diurnal cycling: Observations and models of the upper ocean response to diurnal heating, cooling, and wind mixing. *Journal of Geophysical Research: Oceans*, 91(C7), 8411-8427. doi: 10.1029/JC091iC07p08411
- Roller, C. D., Qian, J.-H., Agel, L., Barlow, M., & Moron, V. (2016). Winter Weather Regimes in the Northeast United States. *Journal of Climate*, 29(8), 2963 - 2980. doi: 10.1175/JCLI-D-15-0274.1

- 818 Schofield, O., Chant, R., Cahill, B., Castelao, R., Gong, D., Kahl, A., ... Glenn,
819 S. (2008). The Decadal View of the Mid-Atlantic Bight from the COOL-
820 room: Is Our Coastal System Changing? *Oceanography*, *21*(4), 108–117. doi:
821 10.5670/oceanog.2008.08
- 822 Yamartino, R. J. (1984). A Comparison of Several "Single-Pass" Estimators of
823 the Standard Deviation of Wind Direction. *Journal of Applied Meteorology*
824 *and Climatology*, *23*(9), 1362 - 1366. doi: 10.1175/1520-0450(1984)023<1362:
825 ACOSPE>2.0.CO;2
- 826 Zielinski, G. A., & Keim, B. D. (2003). *New England Weather, New England Cli-*
827 *mate*. University Press of New England.

Figure 1.

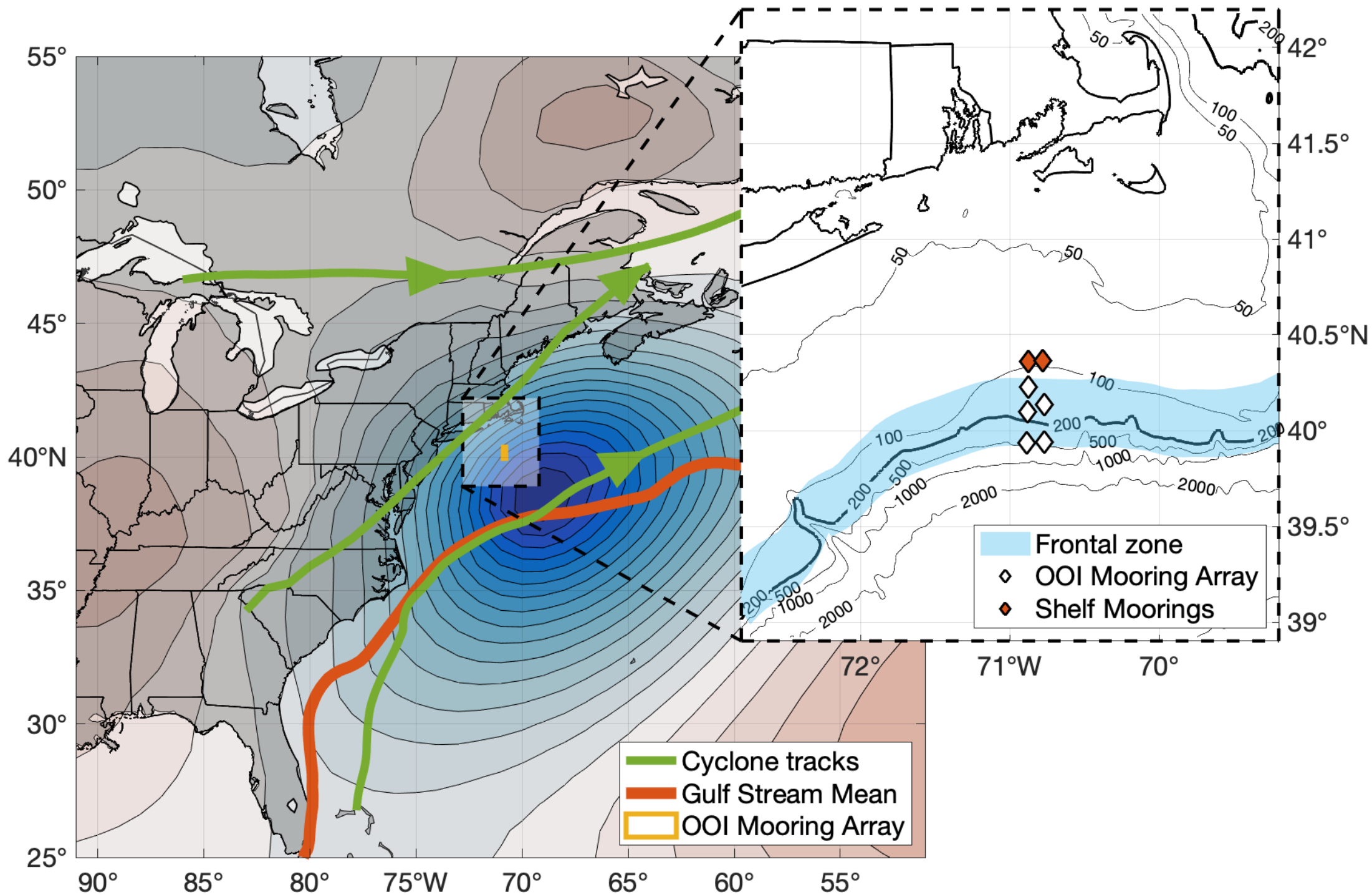


Figure 2.

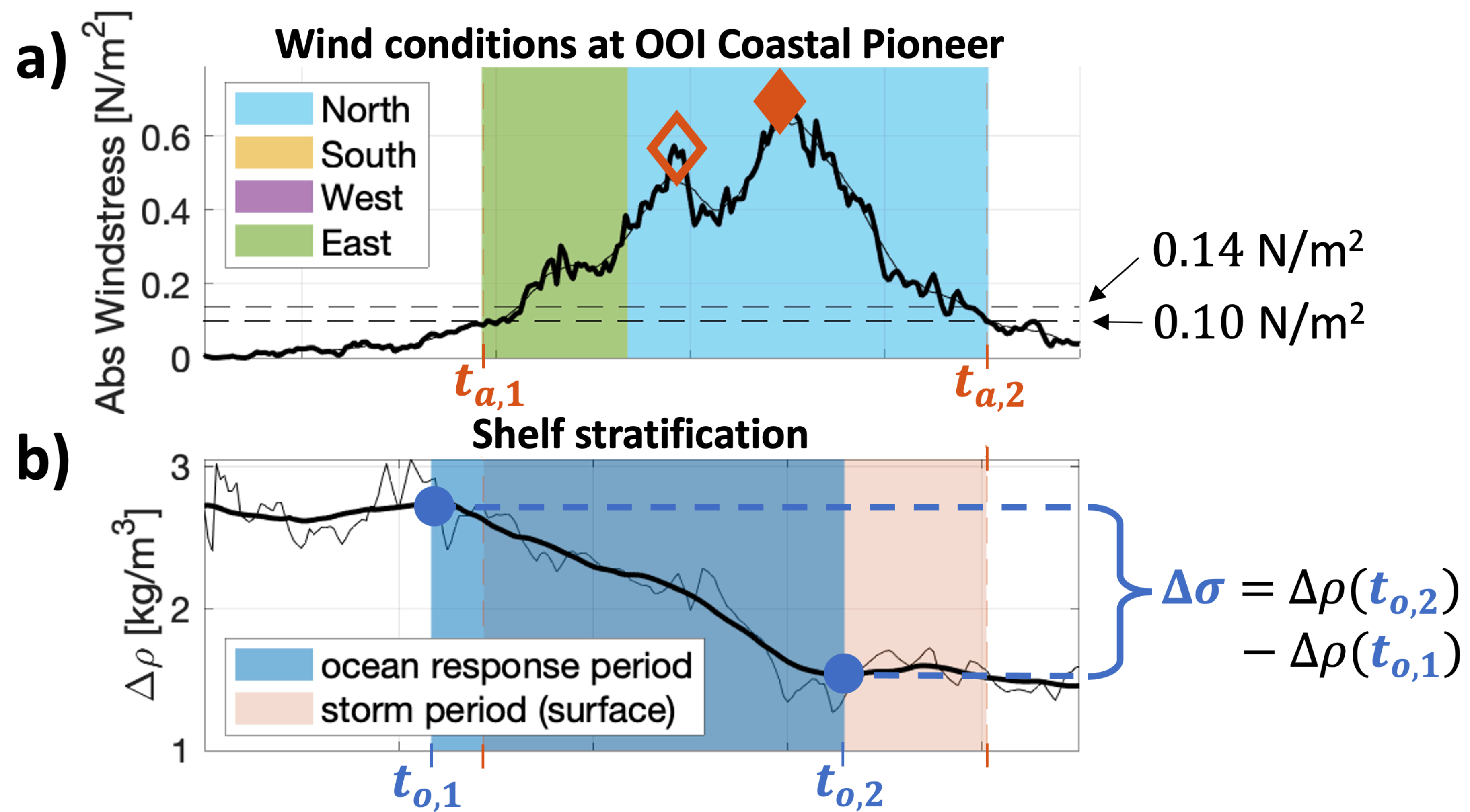


Figure 3.

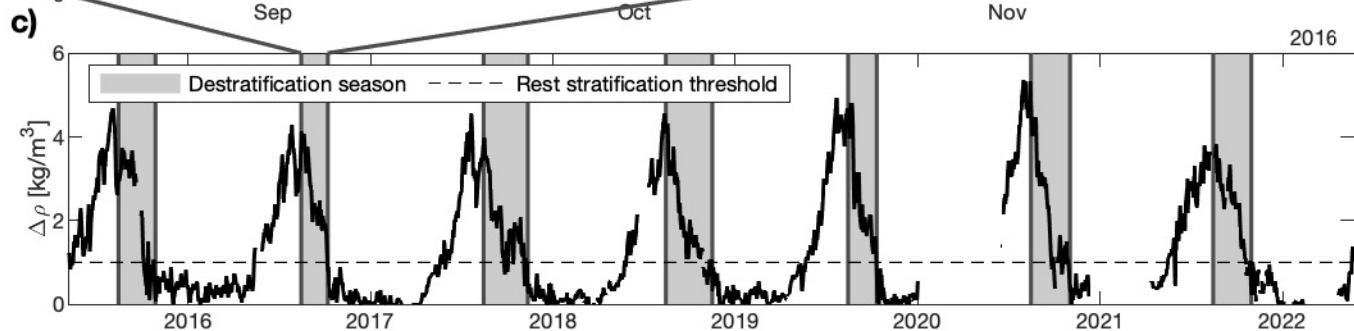
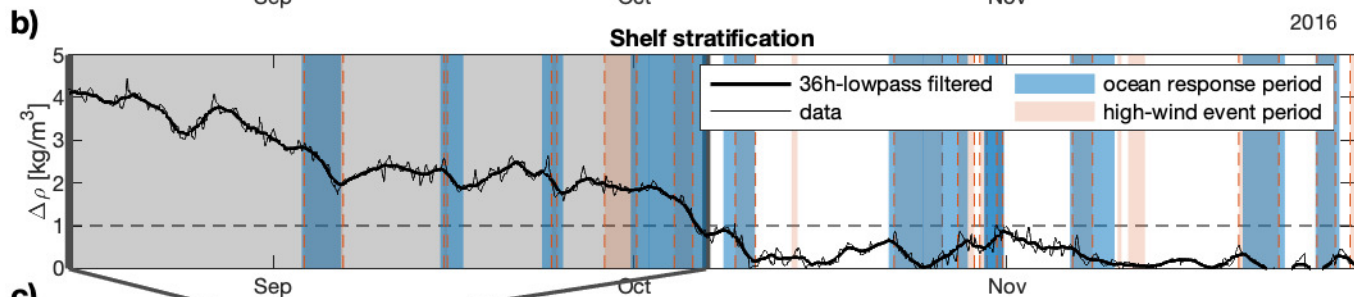
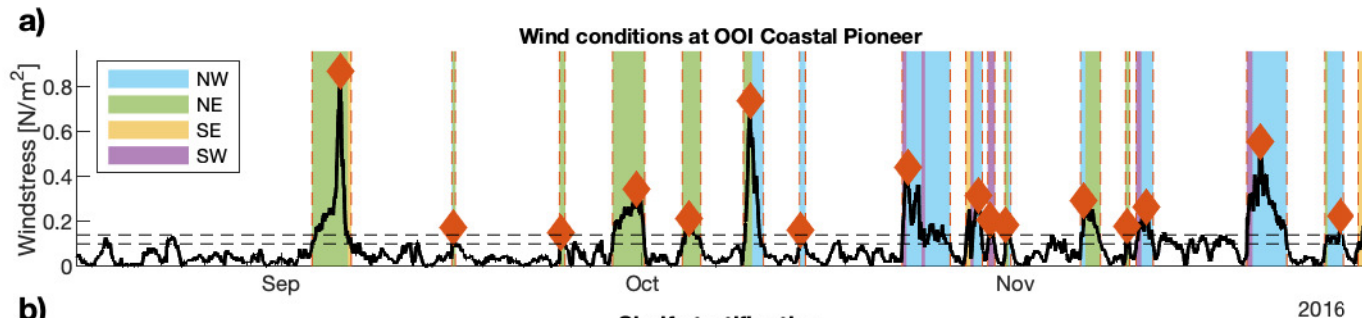


Figure 4.

Figure 5.

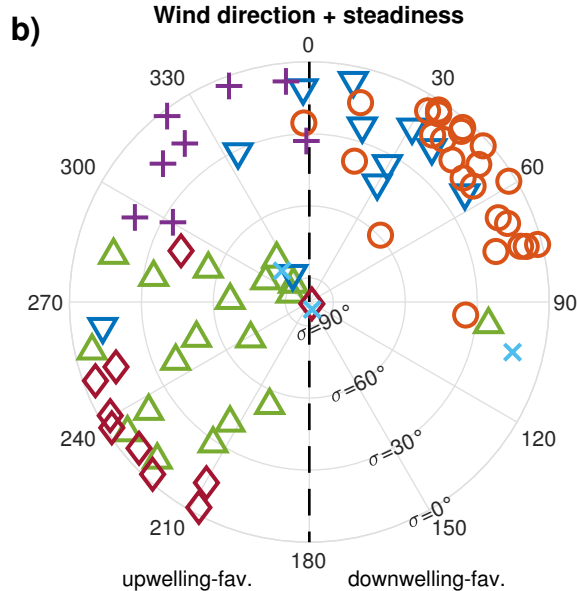
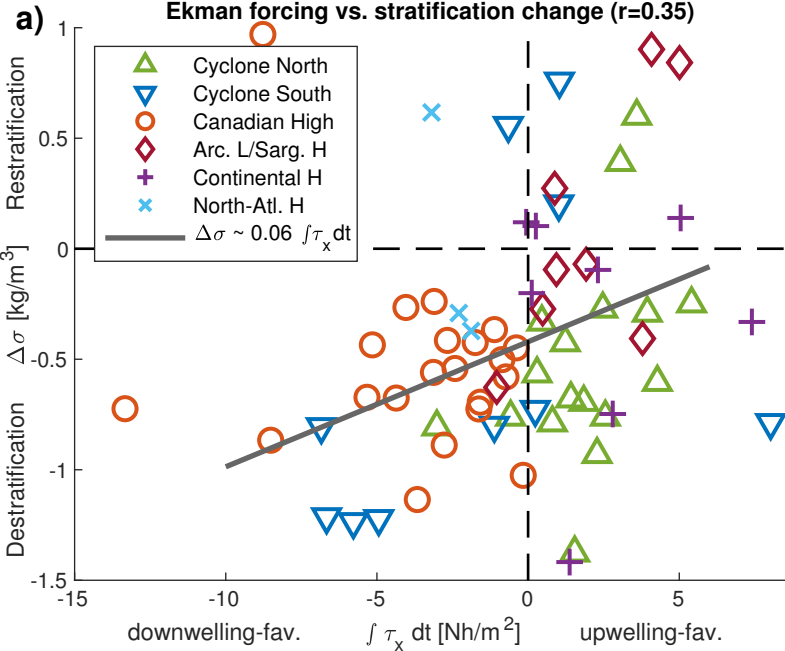


Figure 6.

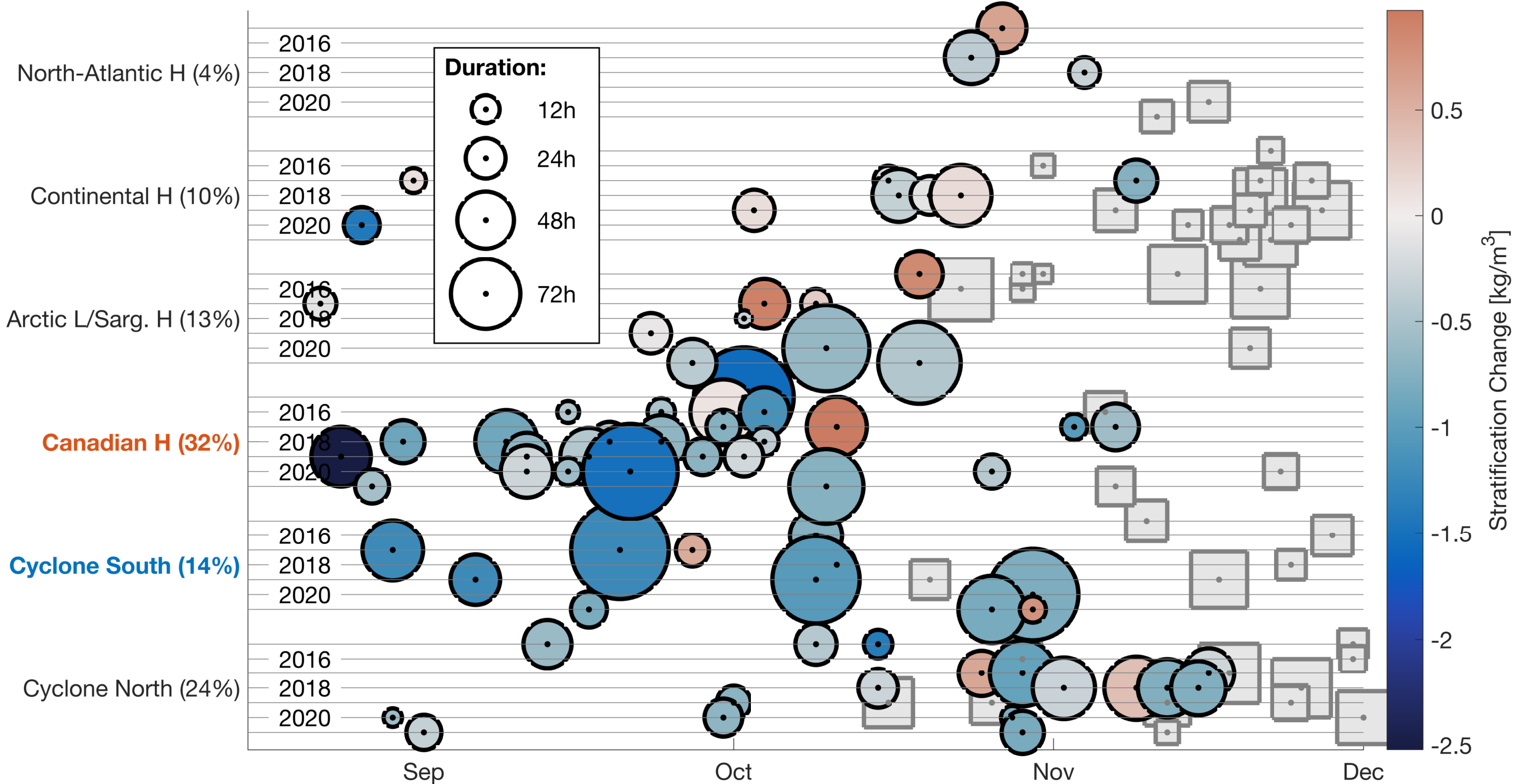


Figure 7.

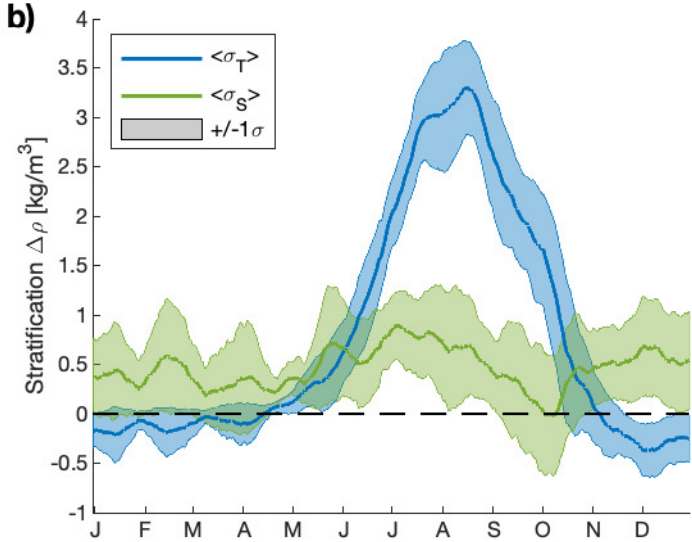
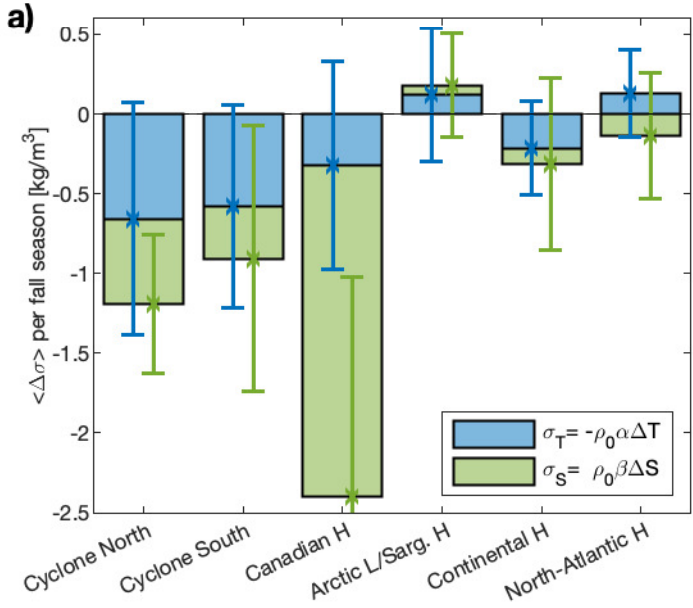


Figure 8.

1D vs. 2D-destratification

